LU TP 09-28
MCnet/09/16
November 2009

Multiparton Interactions and Rescattering*

R. Corke[1] and T. Sjöstrand[2]

Department of Theoretical Physics,
Lund University,
Sölvegatan 14A,
S-223 62 Lund, Sweden

Abstract

The concept of multiple partonic interactions in hadronic events is vital for the understanding of both minimum-bias and underlying-event physics. The area is rather little studied, however, and current models offer a far from complete coverage, even of the effects we know ought to be there. In this article we address one such topic, namely that of rescattering, where an already scattered parton is allowed to take part in another subsequent scattering. A framework for rescattering is introduced for the Pythia 8 event generator and fully integrated with normal multiparton interactions and initial- and final-state radiation. Using this model, the effects on event structure are studied, and distributions are shown both for minimum-bias and jet events.

*Work supported by the Marie Curie Early Stage Training program "HEP-EST" (contract number MEST-CT-2005-019626) and in part by the Marie Curie RTN "MCnet" (contract number MRTN-CT-2006-035606)

[1]richard.corke@thep.lu.se
[2]torbjorn@thep.lu.se

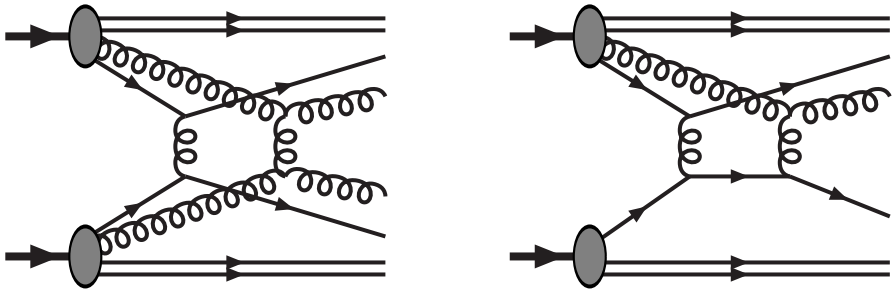

(a) (b)

Figure 1: (a) Two $2 \to 2$ scatterings, (b) a $2 \to 2$ scattering followed by a rescattering

1 Introduction

The run-up to the start of the Large Hadron Collider (LHC) has led to a greatly increased interest in the physics of multiparton interactions (MPI) in hadronic collisions (alternatively called MI for multiple interactions or MPPI for multiple parton–parton interactions in the literature). The concept of MPI has its roots in ideas that preceded QCD, and generators based on MPI have been used for decades to predict LHC physics. It is only in very recent years that the tenets of MPI have caught on in a broader experimental and theoretical community, however, as being central aspects for the proper QCD understanding of collider physics, and not only as handy parameterisations of some unknown physics. At the same time their role as a potentially limiting factor in searches and precision measurements has become more apparent.

The complexity of MPI physics makes purely analytical studies of limited validity, and event generators are often the only way to make contact with data. Existing generators only work within a rather restricted framework, intended to catch the main aspects, but setting aside a number of subleading effects. For instance, existing implementations for hadron–hadron collisions are based on the assumption of disjoint pairwise scatterings, i.e. multiple $2 \to 2$ processes, Fig. 1a. The objective of the current article is to relax this particular constraint; to introduce a formalism that describes rescattering, i.e. where one parton may undergo successive collisions against several other partons, in the simplest case leading to a $3 \to 3$ process, Fig. 1b. This formalism will be integrated into a framework for MPI, initial-state radiation (ISR) and final-state radiation (FSR), where everything can be viewed as a part of a combined evolution process.

Before presenting this complex framework, however, it is necessary to introduce the various building blocks. In Section 2 the main physics principles of MPI are described, and the current experimental status summarised. In Section 3 we zoom in on the existing MPI model in Pythia 8, focusing on the aspects relevant for the modeling of rescattering. In Section 4 rescattering is discussed further, and the details of the new implementation in Pythia 8 are given. Results for a range of different observables are given in Section 5, before a summary and outlook is presented in Section 6.

2 Multiparton Interaction Physics

LHC events will typically contain hundreds of outgoing particles. Some events will contain high-$p_\perp$ objects — partons, photons, leptons, neutrinos, ... — suggestive of a hard-scattering process at large virtuality, while others will not, i.e. all particle production occurs at small $p_\perp$ scales, say around or below 1 GeV. The dividing line is not clearcut, however. As the lower cutoff $p_{\perp\min}$ is reduced, the jet rate continuously increases, until eventually all particles in all events belong to a jet. Well before this stage, the direct relationship of a jet to a high-$p_\perp$ object is gone.

Nevertheless, there is a problem; perturbative QCD not only predicts a large number of jets per event, but an infinite number. The diverging jet cross section is readily visible in the cross section for $2 \to 2$ QCD processes

$$\frac{\mathrm{d}\sigma}{\mathrm{d}p_\perp^2} = \sum_{i,j} \int \mathrm{d}x_1 \int \mathrm{d}x_2 \, f_i(x_1, Q^2) \, f_j(x_2, Q^2) \, \frac{\mathrm{d}\hat{\sigma}}{\mathrm{d}p_\perp^2} \, , \tag{1}$$

where $\mathrm{d}\hat{\sigma}/\mathrm{d}p_\perp^2$ contains a $1/p_\perp^4$ divergence from t-channel gluon exchange (Rutherford scattering), further steepened by the rise of the parton densities f_i, f_j at small x. Part of the solution should be that perturbation theory must break down when $p_\perp$ becomes of order Λ_{QCD}, or equivalently of inverse hadronic size. Another part is to note that eq. (1) is an inclusive cross section which does not tell how scatterings are distributed inside physical events. The task of an MPI model is therefore to regularise the divergence at $p_\perp \to 0$ by nonperturbative effects and recast the remaining jet cross section into a probability for an event to contain one or several $2 \to 2$ subprocesses in various configurations.

Historically, MPI was originally studied in two different contexts (see [1] for a longer survey with references):

1. By the exchange of multiple Pomerons. Translated into QCD language, a cut Pomeron can be viewed as the transfer of a zero-momentum gluon between the two colliding hadrons, transforming them into coloured outgoing beam remnants. Colour fields are stretched longitudinally in between, and eventually fragment to give low-$p_\perp$ particles. Thus, one obtains a model e.g. for multiplicity and rapidity distributions, but without any jets.

2. By the perturbative calculation of two or more (semi-)hard collisions, thus contributing to the rate of multijets with specific jet correlation signatures, but without any underlying events.

These two approaches first came together in a model [2] that extended the perturbative picture to such low $p_\perp$ scales that one could view all events as containing one or more interactions. These interactions would fill the function of cut Pomerons, giving rise to colour fields that stretch across the event and hadronise to give the observable final state. The twist is that now these fields could also stretch out to partons of varying $p_\perp$, thereby giving a smooth transition to (mini)jets, and a unified picture of minimum-bias (MB) and underlying-event (UE) physics. The main parameter of the model is a "colour-screening" $p_{\perp 0}$ scale that is used to dampen the QCD $1/p_\perp^4$ divergence to $1/(p_{\perp 0}^2 + p_\perp^2)^2$. The modeling also involves varying impact parameters (with central collisions likely to involve more activity than peripheral ones), corrected parton densities (to ensure momentum conservation), a

possibility of colour reconnection (to ensure a rising $\langle p_\perp \rangle (n_{\rm charged})$), and a few other aspects. It was implemented in the PYTHIA event generator [3, 4].

For a number of years the model remained unchanged, but in recent years it has been improved. For instance, the original model only treated the highest $p_\perp$ interaction in full, limiting subsequent ones to give $\mathrm{q\overline{q}}$ or gg final states without any showers. With the introduction of junction fragmentation it became possible to handle more complicated beam remnants and thus to consider arbitrary colliding flavour combinations [1], including showers for all interactions. The subsequent introduction of $p_\perp$-ordered showers [5], instead of the older virtuality-ordered ones, allowed a common interleaved evolution of MPI and ISR downwards in $p_\perp$, one of the points being to take into account the competition for beam momentum between these two components. An annealing algorithm for colour reconnection among final-state partons [6] complements the picture of the most sophisticated versions available in PYTHIA 6.4, but also the older options are available for backwards compatibility.

The C++-based PYTHIA 8.1 [7] does away with many older options. It retains the newer beam-remnant handling and the $p_\perp$-ordered showers, now also with FSR interleaved in the common $p_\perp$-ordered evolution sequence by default. It allows for a broader range of $2 \to 2$ processes to be included in the MPI framework, with outgoing photons, leptons, J/ψ and Υ possible, to allow a more realistic mix of possible background processes. Another new feature is the ability to select the nature not only of the hardest subcollision in an event but also of the second hardest. The current colour reconnection algorithm is less flexible than the annealing one in PYTHIA 6.4, however. More details on the PYTHIA 8.1 framework are found in the subsequent sections.

The PHOJET generator [8] has its historical roots in the cut Pomeron approach, with the original soft interactions complemented with a hard $2 \to 2$ component. Thus, an unmodified perturbative component is applied down to a cutoff scale, $p_{\perp\rm min}$, while below this, the soft nonperturbative component takes over. In practice the difference to PYTHIA's single dampened perturbative component is minor, since the region around or below $p_{\perp\rm min}/p_{\perp 0}$ does not give rise to visible jets. PHOJET has an eikonal description of the impact-parameter picture and a component that allows diffraction to be handled as an integrated part of the MPI framework.

One of the simplest ways of simulating the MB and UE activity is through a parameterisation of the main aspects of the data, such as that of UA5 [9]. The emphasis here is on the charged multiplicity distribution and its pseudorapidity distribution. This model was later implemented in the HERWIG event generator [10]. Although such parameterisations can be tuned to describe some distributions well, they are not reliable when extrapolated beyond the fit region, and fail to describe correlations and fluctuations. The JIMMY add-on [11] for HERWIG uses an eikonal model and shares many features both with PHOJET and with the original PYTHIA model. It is only a model for underlying events, however. The model was further extended to include soft interactions in [12], and it is this latter model that forms the basis of the MPI model in HERWIG++ [13].

The most obvious prediction of the MPI approach is that there should be a subsample of events that contains two separate $2 \to 2$ subcollisions, known as double parton scattering (DPS). Experimentally, the problem is that a four-jet sample can contain a significant fraction of $2 \to 4$ events, so-called double bremsstrahlung (DBS). The fall-off of the MPI cross section is steeper than that of bremsstrahlung, so that DPS is dominant only at rather

small $p_\perp$ scales. The trick is therefore to do the analysis with as low $p_{\perp\min}$ thresholds as possible, while still keeping the jets sufficiently hard that the jet momentum can reasonably well be associated with that of an originating parton. In this way one can study kinematical distributions that distinguish DPS and DBS events, such as that the former ought to consist of two parton pairs lined up back-to-back in azimuth. The first measurement of this kind was performed by the AFS collaboration at ISR [14]. So far, the clearest observation has been provided by the CDF collaboration in a study of $\gamma + 3$ jet events [15]. Recently a preliminary D0 study [16] of the same channel confirms the CDF results with even more statistics.

More indirect evidence comes from a number of other observables, starting from the fact that observed multiplicity distributions are much broader than can easily be understood in terms of only one interaction per event, but are well explained by a varying number of MPI. This variation can also explain the observed strong forward–backward correlations in multiplicity.

The CDF studies on MB and UE activity [17–21] are also well known. These study, in detail, the old UA1 "pedestal effect" observation [22] that the activity in events triggered by the presence of a high-$p_\perp$ jet is much higher, also well away from the jets, than in the bulk of normal events. The rise of this activity is very steep up to a jet $p_\perp$ of roughly 10 GeV, and thereafter rises only very slowly. The latter rise can be attributed to contributions from ISR and FSR, while the sudden change of behaviour at around 10 GeV is a feature of MPI models with an impact-parameter dependence.

Since not all aspects of the models can be derived from first principles there are a number of parameters that have to be tuned to data, such as those in the MPI, ISR, FSR, beam-remnant and hadronisation frameworks. Therefore the tuning and testing of these models go hand in hand. A well-known example is the tunes of R.D. Field [18,19,21], such as Tune A and Tune DW, originally intended for the CDF collaboration but with widespread usage. These are based on the older Pythia models, while the Perugia [23] and Professor [24] tunes are for the most recent Pythia 6.4 models. Other tunes have been developed inside experimental collaborations [25].

These tunes are used to try to get an insight into what can be expected at new experiments, specifically at the LHC. Such extrapolations, however, come with a high level of uncertainty; within many of the models in a generator there are parameters with an unknown energy scaling. There is, therefore, also the exciting prospect that new data will further constrain and improve models, as well as revealing new insights. MPI is one of the least well understood areas. While current models, after tuning, are able to describe many distributions very well, there are still many others which are not fully described. This is a clear sign that new physics aspects need to be introduced, and it is therefore not enough to "sit still" while waiting for new data. It is with this in mind that we look at rescattering, where an already scattered parton is able to undergo another subsequent scattering. Such processes have been studied analytically already many years ago, notably by Paver and Treleani [26]. There, estimates were given for the size of rescattering effects based on a set of ansätze for the calculation of parton distribution functions (PDFs). As with MPI in general, although such rescatterings may be relatively soft, they can lead to non-trivial colour flows which can change the structure of events.

The theoretical study of MPI and rescattering, in various approaches, has received renewed attention in recent years [27–32].

The experimental study can be traced at least back to the so-called Cronin effect [33]. The observation is that in proton-nucleus collisions the "high-$p_\perp$" particle production is enhanced and the low-$p_\perp$ one reduced, relative to a simple (geometrical) rescaling of the proton-nucleon production rates. The interpretation is not unambiguous, but some form of rescattering is likely to be involved, whether at the parton or at the hadron level. Rescattering is nowadays taken for granted in the study of heavy-ion collisions at RHIC, say, for instance as an important aspect of the initial formation of a quark–gluon plasma. In this busy environment it is not possible to study the individual rescattering processes, however, but only to deduce their collective importance.

To the best of our knowledge, a model for the detailed effects of rescattering in hadron–hadron collisions has never before been published. It is precisely the task of this article to present a first such complete model, formulated in the context of the Pythia 8 event generator, fully taking into account all other aspects of complete events, including hard processes, initial- and final-state radiation, colour flow, and hadronisation. This program is publicly available. It thus invites experimental tests, not restricted by the imagination of the current authors, but by that of the experimental community.

3 Multiparton Interactions in Pythia 8

We begin this section by reviewing the existing MPI framework present in Pythia 8, with special attention paid to the areas which will later be affected by the introduction of rescattering. For a more comprehensive discussion, readers are directed to [4] and the references therein. There are some aspects, like the complete interleaving of ISR, FSR and MPI and the related dipole structure of radiation, that are new to Pythia 8 and are presented here for the first time.

The master equation for the new interleaved evolution is

$$\begin{aligned}\frac{\mathrm{d}\mathcal{P}}{\mathrm{d}p_\perp} &= \left(\frac{\mathrm{d}\mathcal{P}_{\mathrm{MPI}}}{\mathrm{d}p_\perp} + \sum \frac{\mathrm{d}\mathcal{P}_{\mathrm{ISR}}}{\mathrm{d}p_\perp} + \sum \frac{\mathrm{d}\mathcal{P}_{\mathrm{FSR}}}{\mathrm{d}p_\perp}\right) \\ &\times \exp\left(-\int_{p_\perp}^{p_{\perp i-1}} \left(\frac{\mathrm{d}\mathcal{P}_{\mathrm{MPI}}}{\mathrm{d}p'_\perp} + \sum \frac{\mathrm{d}\mathcal{P}_{\mathrm{ISR}}}{\mathrm{d}p'_\perp} + \sum \frac{\mathrm{d}\mathcal{P}_{\mathrm{FSR}}}{\mathrm{d}p'_\perp}\right) \mathrm{d}p'_\perp\right) . \qquad (2)\end{aligned}$$

Here $p_\perp = p_{\perp i}$ is the transverse momentum of the i^{th} interaction or shower branching to take place, with a combined Sudakov-like form factor expressing that nothing happens between the previous $(i-1)^{th}$ interaction/branching and the current one.

The physics content of this equation is as follows. A hard process occurs at a scale $p_{\perp\mathrm{hard}} = p_{\perp 1}$. At a scale $p_{\perp 2} < p_{\perp 1}$ either there is a second hard interaction, one of the incoming partons radiates, or one of the outgoing partons radiates. The respective probability for each of these to occur at a generic scale $p_\perp$ is schematically designated $\mathrm{d}\mathcal{P}_{\mathrm{MPI}}/\mathrm{d}p_\perp$, $\mathrm{d}\mathcal{P}_{\mathrm{ISR}}/\mathrm{d}p_\perp$, and $\mathrm{d}\mathcal{P}_{\mathrm{FSR}}/\mathrm{d}p_\perp$, respectively. Their sum gives the total probability for something to happen at $p_\perp$. The requirement that $p_{\perp 2}$ is the second hardest scale implies that nothing happened in the range $p_{\perp 1} > p_\perp > p_{\perp 2}$. Assuming that the no-activity probability factorises, $\mathcal{P}_{\mathrm{no}}(p_{\perp 1} > p_\perp > p_{\perp 2}) = \mathcal{P}_{\mathrm{no}}(p_{\perp 1} > p_\perp > p_\perp{}') \times \mathcal{P}_{\mathrm{no}}(p_\perp{}' > p_\perp > p_{\perp 2})$, and conservation of probability then gives the exponential in the above expression.

The story now repeats for the next scale, $p_{\perp 3} < p_{\perp 2}$. If the previous step gave an MPI then there are two systems, either of which can undergo ISR or FSR. If instead it gave

an ISR or FSR then the number of final-state partons of that system increased by one. Therefore, in either case, the sums in eq. (2) run over an increased number of partons. Furthermore, several partons may have obtained changed momenta, e.g. by recoil effects from an ISR emission, and the momentum in the beam remnants may have been reduced and their flavour composition changed. There are thus several reasons why the probability expressions in eq. (2) change at the $p_{\perp 2}$ scale; the simple notation of eq. (2) hides a lot of complexity.

In summary, for each new lower $p_\perp$ scale there is one more scattering subsystem or one more outgoing parton in an existing subsystem. The sequence extends until some lower cutoff is reached, which may be different for the three components. Below this scale the probability is set to zero, and the $p_\perp$ sequence terminates. A smooth turnoff would be more realistic than a sharp cutoff, but the principle is the same.

One important aspect of the interleaved evolution is that it introduces an element of competition, specifically that the remaining pool of beam-remnant momentum is gradually reduced, and therefore the phase space for new interactions or emissions shrinks correspondingly. One could contrast our approach with two alternatives. In one extreme each interaction is allowed to shower in full before the next interaction is considered. In that case one tends to get fewer interactions, with each interaction having more activity, especially the first one. In the other extreme all interactions are found before showers are added, which then gives more interactions per event with less radiation for each. Differences should not be exaggerated, however, since most of the momentum remains in the remnants for the majority of events.

It would be tempting to view the ordering in terms of decreasing $p_\perp$ as one of increasing time, in the spirit of the Heisenberg uncertainty principle. This would be too simpleminded, however. MPI are supposed to occur when the two (more or less) Lorentz contracted hadron "pancakes" pass through each other, and if so, the different MPI's occur simultaneously rather than in any causal order. At that time the ISR should already "be there", in terms of virtual fluctuations that are put on the mass shell by the collisions. Here, time stretches backwards, with low-$p_\perp$ fluctuations able to live longer and thus be produced earlier than high-$p_\perp$ ones. So it is only for FSR that formation time arguments gives the desired answer. Instead we would like to view eq. (2) primarily as an expression of conditional probabilities; *given* that we already know the event structure if viewed at some resolution scale $p_\perp$, what further activity is allowed and with what rate at a lower $p_\perp$ resolution? In this sense we are zooming in on an event that is "already" there, only resolving finer and finer details. At larger scales the system is still simple, and so perturbation theory should provide a good answer. At lower scales the event complexity mounts and so further modeling becomes increasingly difficult, but then again these details will play a lesser role. Of course, implicit in this is that we already know that $p_\perp$ ordering is a sensible choice for ISR, FSR and MPI individually, and thus presumably for the combination of the three.

A final, technical note on eq. (2). It would seem to be a major task to generate events according to this non-trivial expression that can sum over many terms, each with a lot of complexity. However, there is a simple solution, "the winner takes it all". The idea is that each term individually is used to find a $p_\perp$ scale, with Monte Carlo methods, and then the one with largest $p_\perp$ is selected to occur. We illustrate this with simplified notation and

only two probabilities, $\mathcal{P}_a(t)$ and $\mathcal{P}_b(t)$, with t increasing:

$$\begin{aligned}\mathcal{P}(t) &= (\mathcal{P}_a(t)+\mathcal{P}_b(t)) \times \exp\left(-\int_{t_{i-1}}^{t}(\mathcal{P}_a(t')+\mathcal{P}_b(t'))\,\mathrm{d}t'\right)\\ &= \left[\mathcal{P}_a(t)\,\exp\left(-\int_{t_{i-1}}^{t}\mathcal{P}_a(t')\mathrm{d}t'\right)\right]\times\exp\left(-\int_{t_{i-1}}^{t}\mathcal{P}_b(t')\mathrm{d}t'\right)\\ &+ \left[\mathcal{P}_b(t)\,\exp\left(-\int_{t_{i-1}}^{t}\mathcal{P}_b(t')\mathrm{d}t'\right)\right]\times\exp\left(-\int_{t_{i-1}}^{t}\mathcal{P}_a(t')\mathrm{d}t'\right)\ . \end{aligned} \tag{3}$$

Here the expression inside the first square brackets is the probability to select a $t_a = t_i$ according to $\mathcal{P}_a$ alone, as can be done e.g. with the veto algorithm [4], while the subsequent factor is the probability that $\mathcal{P}_b$ did *not* pick a t_b in the range $t_{i-1} < t_b < t_a$. That is, that a is picked and $t_a < t_b$, while correspondingly the last term is the probability that b is picked and $t_b < t_a$. From here it is easy to generalise to the original task.

3.1 Multiparton Interactions

If we now focus on just the contribution from MPI, the probability for an interaction is given by

$$\frac{\mathrm{d}\mathcal{P}_{\mathrm{MPI}}}{\mathrm{d}p_\perp} = \frac{1}{\sigma_{nd}}\frac{\mathrm{d}\sigma}{\mathrm{d}p_\perp}\ \exp\left(-\int_{p_\perp}^{p_{\perp i-1}}\frac{1}{\sigma_{nd}}\frac{\mathrm{d}\sigma}{\mathrm{d}p'_\perp}\mathrm{d}p'_\perp\right), \tag{4}$$

where σ_{nd} is the non-diffractive inelastic cross section and $\mathrm{d}\sigma/\mathrm{d}p_\perp$ is given by the perturbative QCD $2 \to 2$ cross section in non-diffractive events (we leave the issue of diffractive events aside for this article). This cross section is dominated by t-channel gluon exchange, and diverges roughly as $\mathrm{d}p_\perp^2/p_\perp^4$. To avoid this divergence, the idea of colour screening is introduced. The concept of a perturbative cross section is based on the assumption of free incoming states, which is not the case when partons are confined in colour-singlet hadrons. One therefore expects a colour charge to be screened by the presence of nearby anti-charges; that is, if the typical charge separation is d, gluons with a transverse wavelength $\sim 1/p_\perp > d$ are no longer able to resolve charges individually, leading to a reduced effective coupling. This is introduced by reweighting the interaction cross section such that it is regularised according to

$$\frac{\mathrm{d}\hat{\sigma}}{\mathrm{d}p_\perp^2} \propto \frac{\alpha_{\mathrm{s}}^2(p_\perp^2)}{p_\perp^4} \to \frac{\alpha_{\mathrm{s}}^2(p_{\perp 0}^2+p_\perp^2)}{(p_{\perp 0}^2+p_\perp^2)^2}, \tag{5}$$

where $p_{\perp 0}$ (related to $1/d$ above) is now a free parameter in the model. To be more precise, it is the physical cross section $\mathrm{d}\sigma/\mathrm{d}p_\perp^2$ that needs to be regularised, i.e. the convolution of $\mathrm{d}\hat{\sigma}/\mathrm{d}p_\perp^2$ with the two parton densities, eq. (1). One is thus at liberty to associate the screening factor with the incoming hadrons, half for each of them, instead of with the interaction. Such an association also gives a recipe to regularise the ISR divergence, which goes like $\alpha_{\mathrm{s}}(p_\perp^2)/p_\perp^2$.

Not only $p_{\perp 0}$ itself, as determined e.g. from Tevatron data, comes with a large uncertainty, but so does the energy scaling of this parameter. The ansatz for the energy dependence of $p_{\perp 0}$ is that it scales in a similar manner to the total cross section, i.e. driven by an effective power related to the Pomeron intercept [34], which in turn could be related

to the small-x behaviour of parton densities. This leads to a scaling

$$p_{\perp 0}(E_{\mathrm{CM}}) = p_{\perp 0}^{\mathrm{ref}} \times \left(\frac{E_{\mathrm{CM}}}{E_{\mathrm{CM}}^{\mathrm{ref}}} \right)^{E_{\mathrm{CM}}^{\mathrm{pow}}}, \tag{6}$$

where $E_{\mathrm{CM}}^{\mathrm{ref}}$ is some convenient reference energy and $p_{\perp 0}^{\mathrm{ref}}$ and $E_{\mathrm{CM}}^{\mathrm{pow}}$ are parameters to be tuned to data. There is no guarantee that this is the correct shape, however; some studies have suggested that the rise of $p_{\perp 0}$ may flatten out at higher energies [35, 36].

Up to this point, all parton-parton interactions have been assumed to be independent, such that the probability to have n interactions in an event, $\mathcal{P}_n$, is given by Poissonian statistics. This picture is now changed, first by requiring that there is at least one interaction, such that we have a physical event, and second by including an impact parameter, b. For a given matter distribution, $\rho(r)$, the time-integrated overlap of the incoming hadrons during collision is given by

$$\mathcal{O}(b) = \int \mathrm{d}t \int \mathrm{d}^3x \; \rho(x, y, z) \; \rho(x + b, y, z + t), \tag{7}$$

after a suitable scale transformation to compensate for the boosted nature of the incoming hadrons.

Such an impact parameter picture has central collisions being generally more active, with an average activity at a given impact parameter being proportional to the overlap, $\mathcal{O}(b)$. While requiring at least one interaction results in $\mathcal{P}_n$ being narrower than Poissonian, when the impact parameter dependence is added, the overall effect is that $\mathcal{P}_n$ is broader than Poissonian. The addition of an impact parameter also leads to a good description of the "Pedestal Effect", where events with a hard scale have a tendency to have more underlying activity; this is as central collisions have a higher chance both of a hard interaction and of more underlying activity. This centrality effect naturally saturates at $p_{\perp hard} \sim 10\,\mathrm{GeV}$ or, more specifically, when $\sigma_{\mathrm{jet}}(p_\perp > p_{\perp hard}) \ll \sigma_{\mathrm{nd}}$ [2].

ISR, FSR and MPI can all lead to changes in the incoming PDFs. With FSR, a colour dipole can stretch from a radiating parton to a beam remnant, leading to (a modest amount of) momentum shuffling between the beam and the parton. Both ISR and MPI can result in large x values being taken from the beams, as well as leading to flavour changes in the PDFs.

In the original model, PDFs were rescaled only such that overall momentum was conserved. This was done by evaluating PDFs at a modified x value

$$x_i' = \frac{x_i}{1 - \sum_{j=1}^{i-1} x_j}, \tag{8}$$

where the subscript i refers to the current interaction and the sum runs over all previous interactions. The current model still conserves momentum, but does it in a more flavour-specific manner, as follows. If a valence quark is taken from one of the incoming hadrons, the valence PDF is rescaled to the remaining number. If, instead, a sea quark ($\mathrm{q_s}$) is taken from a hadron, an anti-sea companion quark ($\mathrm{q_c}$) is left behind. The x distribution for this companion quark is generated from a perturbative ansatz, where the sea/anti-sea quarks are assumed to have come from a gluon splitting, $\mathrm{g} \to \mathrm{q_s q_c}$. Subsequent perturbative evolution of the $\mathrm{q_c}$ distribution is neglected. Note that if a valence quark is removed from a PDF,

momentum must be put back in, while if a companion quark is added, momentum must be taken from the PDF, in order to conserve momentum overall.This is done by allowing the normalisation of the sea and gluon PDFs to fluctuate.

3.2 Initial- and Final-State Radiation

As this framework now includes radiation from all MPI scattering systems, we will later need to consider radiation from systems that have an incoming rescattering parton. For this reason, we take some time to briefly review the parton shower algorithm, including some details of recoil kinematics.

Both initial and final-state radiation are governed by the DGLAP equations [37]

$$\mathrm{d}\mathcal{P}_a(z,t) = \frac{\mathrm{d}t}{t}\,\frac{\alpha_\mathrm{s}}{2\pi}\,P_{a\to bc}(z)\,\mathrm{d}z\ , \tag{9}$$

giving the probability that a parton a will branch into partons b and c at some scale t, with parton b taking fraction z of the energy of a and parton c a fraction $(1-z)$. The splitting kernels $P_{a\to bc}(z)$ give the universal collinear limit of the matrix-element expressions for $\mathrm{q}\to\mathrm{qg}$, $\mathrm{g}\to\mathrm{gg}$ and $\mathrm{g}\to\mathrm{q\overline{q}}$ branchings. Within the parton shower, an ordering is introduced through a Sudakov form factor [38]

$$\mathcal{P}_a^\mathrm{no}(t_\mathrm{max},t) = \exp\left(-\int_t^{t_\mathrm{max}}\int_{z_\mathrm{min}}^{z_\mathrm{max}}\mathrm{d}\mathcal{P}_a(z',t'^2)\right)\ , \tag{10}$$

which unitarises the naïve splitting probability given by the DGLAP equations. Picking the evolution variable t to be the squared transverse momentum (described below), the overall emission probability is given by

$$\mathrm{d}\mathcal{P}_a = \frac{\mathrm{d}p_\perp^2}{p_\perp^2}\,\frac{\alpha_\mathrm{s}(p_\perp^2)}{2\pi}\,P_{a\to bc}(z)\,\mathrm{d}z\,\mathcal{P}_a^\mathrm{no}(p_{\perp\mathrm{max}}^2,p_\perp^2)\ , \tag{11}$$

where we note that the scale choice for α_s is selected to be $p_\perp^2$ independently of the choice of the evolution variable. This formulation is already suitable for final-state showers, where outgoing partons may have timelike virtualities that evolve downwards towards on-shell partons. For ISR, however, the partons build up increasingly spacelike virtualities as they approach the interaction point. In this scenario, it is customary to use backwards evolution [39, 40], where an already selected parton b may become unresolved into a parton a, given by an overall probability

$$\mathrm{d}\mathcal{P}_b = \frac{\mathrm{d}p_\perp^2}{p_\perp^2}\,\frac{\alpha_\mathrm{s}(p_\perp^2)}{2\pi}\,\frac{x'f_a(x',p_\perp^2)}{xf_b(x,p_\perp^2)}\,P_{a\to bc}(z)\,\mathrm{d}z\,\mathcal{P}_b^\mathrm{no}(x,p_{\perp\mathrm{max}}^2,p_\perp^2)\ , \tag{12}$$

where now also the Sudakov form factor involves the ratio of parton densities.

The $p_\perp^2$ evolution variable can be related to the virtuality Q^2 by considering the lightcone kinematics ($p^\pm = E \pm p_z$) of a parton a moving along the $+z$ axis, splitting into parton b with $p_b^+ = zp_a^+$ and parton c with $p_c^+ = (1-z)p_a^+$. Conservation of p_- then gives

$$p_\perp^2 = z(1-z)m_a^2 - (1-z)m_b^2 - zm_c^2\ . \tag{13}$$

For final state radiation, $Q^2 = m_a^2$ with $m_b = m_c = 0$, while for initial state radiation, $Q^2 = -m_b^2$ with $m_a = m_c = 0$, giving

$$\begin{aligned} \text{FSR}: \ p_\perp^2 &= z(1-z)Q^2 \ , \\ \text{ISR}: \ p_\perp^2 &= (1-z)Q^2 \ . \end{aligned} \tag{14}$$

The detailed kinematics, to be described below, does not use a lightcone z definition, but rather an energy fraction in a specified reference frame. The Q^2 extracted from eq. (14), together with the new z interpretation, therefore gives a true $p_\perp^2$ slightly smaller than the one above.

An important new feature of the $p_\perp^2$-ordered showers is the approach taken to recoil. This approach is inspired by a cascade formulated in terms of radiation from dipoles, which has been implemented in the ARIADNE program [41]. In this hybrid-dipole approach, each radiating parton has associated with it a recoiler, which together form a dipole. The energy and momentum of this dipole is preserved when a parton, previously on mass shell, is assigned a virtuality. Preliminary kinematics are constructed directly after each branching, such that unevolved partons are always on mass shell.

In the final-state shower evolution, the selection of recoilers is based on colour partners (with colours traced in the $N_C \to \infty$ limit). A gluon, which carries both colour and anti-colour indices, therefore has two recoiling partners, with the emission rate split between them. There are then two further possibilities for selecting the recoiling parton

- Initial state: the recoiler is the parton in the initial state that carries the same (anti-)colour index as the radiator. This dipole configuration implies that the extra momentum required to keep all partons on shell is taken from the beam and as a result will be slightly suppressed by PDF factors.
- Final state: the recoiler is the parton in the final state that carries the opposite (anti-)colour as the radiator (i.e. if the radiator carries colour index i, its recoiler is the parton that carries anti-colour i).

Once a dipole system has been selected to radiate, the kinematics of the new outgoing partons b and c are constructed in the rest frame of the radiator (a) and recoiler (r) system. With the new virtuality given by $Q^2 = m_a^2 = p_\perp^2/z(1-z)$ and $m_{ar}^2 = (p_a + p_r)^2$, the increase in E_a and therefore the decrease in E_r is given by

$$\frac{m_{ar}}{2} \to \frac{(m_{ar}^2 \pm Q^2)}{2m_{ar}} \ . \tag{15}$$

Finally, partons b, c and the new recoiler are boosted back to their original frame.

With the initial-state shower, we are now doing a backwards evolution, where a parton b is resolved as coming from a previous branching $a \to bc$. At any branching scale, there will be two resolved incoming partons to a given interaction, and it is the parton on the other side of the event that is marked as the recoiler. Parton b, previously massless, is now assigned a spacelike virtuality $m_b^2 = -Q^2$ while the dipole mass m_{br} remains unchanged by the branching. Once the kinematics of the branching has been constructed, there is an extra step to be taken; all partons from the original $b + r$ interaction must be boosted and rotated so that it is now parton a that is incoming along the z axis.

Note that this choice is different than in the Catani-Seymour dipole picture [42]. There, the colour flow is used to assign a recoil parton that can be either in the initial state, as

above, or in the final state. The drawback of this approach, which at first glance appears attractive and symmetric with the FSR procedure, can be illustrated with the production process $q\overline{q} \to Z^0$. In a first emission $q \to qg$, indeed the Z^0 takes the $p_\perp$ recoil of the emitted gluon. Thereafter, however, the colour flows from the beams to the gluon, and the Z^0 is not affected by any subsequent emissions. This runs counter to the result of a Feynman-diagrammatic analysis of how the $p_\perp$ of the Z^0 can build up by repeated emissions from the incoming partons. In this case we prefer to stay closer to the latter picture, although this may also have its own shortcomings.

3.3 Beam Remnants, Primordial $k_\perp$ and Colour Reconnection

When the $p_\perp$ evolution has come to an end, the beam remnants will consist of the remaining valence content of the incoming hadrons as well as any companion quarks. These remnants must carry the remaining fraction of longitudinal momentum. PYTHIA will pick x values for each component of the beam remnants according to distributions such that the valence content is "harder" and will carry away more momentum. In the rare case that there is no remaining quark content in a beam, a gluon is assigned to take all the remaining momentum.

The event is then modified to add primordial $k_\perp$. Partons are expected to have a non-zero $k_\perp$ value just from Fermi motion within the incoming hadrons. A rough estimate based on the size of the proton gives a value of $\sim 0.3\,\mathrm{GeV}$, but when comparing to data, for instance the $p_\perp$ distribution of Z^0 at CDF, a value of $\sim 2\,\mathrm{GeV}$ appears to be needed. The current solution is to decide a $k_\perp$value for each initiator parton taken from a hadron based on a Gaussian whose width is generated according to an interpolation

$$\sigma(Q, \widehat{m}) = \frac{Q_{\frac{1}{2}}\,\sigma_{\mathrm{soft}} + Q\,\sigma_{\mathrm{hard}}}{Q_{\frac{1}{2}} + Q}\,\frac{\widehat{m}}{\widehat{m}_{\frac{1}{2}} + \widehat{m}}\ , \tag{16}$$

where Q is the hardness of a sub-collision ($p_\perp$ for a $2 \to 2$ QCD process) and $\widehat{m}$ its invariant mass, σ_{soft} and σ_{hard} is a minimal and maximal value, and $Q_{\frac{1}{2}}$ and $\widehat{m}_{\frac{1}{2}}$ the respective scale giving a value halfway between the two extremes. Beam remnants are assigned a separate width σ_{remn} comparable with σ_{soft}. The independent random selection of primordial $k_\perp$ values gives a net imbalance within each incoming beam, which is shared between all initiator and remnant partons, with a reduction factor $\widehat{m}/(\widehat{m}_{\frac{1}{2}} + \widehat{m})$ for initiators of low-mass systems. With the $k_\perp$'s of the two initiators of a system known, all the outgoing partons of the system can be rotated and Lorentz boosted to the relevant frame. During this process, the invariant mass and rapidity of all systems is maintained by appropriately scaling the lightcone momenta of all initiator partons.

The final step is colour reconnection. In the old MPI framework, good agreement to CDF data is obtained if 90% of additional interactions produces two gluons with "nearest neighbour" colour connections [17]. More recently, an annealing algorithm has been used [6], again requiring a significant amount of reconnection to describe data. In PYTHIA 8 colour reconnection is currently performed by giving each system a probability to reconnect with a harder system

$$\mathcal{P} = \frac{{p_\perp}^2_{Rec}}{({p_\perp}^2_{Rec} + p_\perp^2)}, \qquad p_{\perp Rec} = R \times p_{\perp 0}, \tag{17}$$

where R is a user-tunable parameter and $p_{\perp 0}$ is the same parameter as in eq. (5).

The idea of colour reconnection can be motivated by noting that MPI leads to many colour strings that will overlap in physical space, which makes the separate identity of these strings questionable. Alternatively, moving from the limit of $N_C \to \infty$ to $N_C = 3$, it is not unreasonable to allow these strings to be connected differently due to a coincidence of colour. Adapting either of these approaches, dynamics is likely to favour reconnections that reduce the total string length and thereby the potential energy.

With the above probability for reconnection, it is easier to reconnect low-$p_\perp$ systems, which can be viewed as them having a larger spatial extent, such that they are more likely to overlap with other colour strings. Currently, however, this is only a convenient ansatz. More than that, given the lack of a firm theoretical basis, the need for colour reconnection has only been established within the context of specific models.

3.4 Tuning and Energy Dependence

Pythia contains a large number of parameters, and it is not feasible to attempt to tune them all. Even with the less relevant ones retained at their default values, the task of tuning the rest simultaneously is nontrivial. A simplification is offered by the assumption of jet universality, since then e^+e^- data can be used to tune FSR and hadronisation independently of other aspects. Such a tune exists, closely related to the Professor/Rivet tuning of Pythia 6.4 [24]. With these parameters fixed, a second step is to tune the other aspects, such as ISR and MPI, to hadron collider data. Here, the Pythia 8 models differ enough from the previous versions, that carrying across parameters is non trivial. Until recently, default parameters for these parts of the simulation were based on an early and primitive comparison with data. It is only recently that a somewhat more detailed tune, "Tune 1", has been released, based on the Perugia tunes [23]. Studies have also been made with the Professor/Rivet framework [43], but have not yet resulted in a complete tune.

For MPI, and therefore also for rescattering, the $E_{\rm CM}^{\rm pow}$ parameter of eq. (6) is vital for extrapolating to LHC energies. Prior to Tune 1, a default value of $E_{\rm CM}^{\rm pow} = 0.16$ was chosen, supported by toy model studies [35] and previous tuning efforts [44]. The newer Perugia [23] and Professor tunes [24] now point towards a larger value of $E_{\rm CM}^{\rm pow} = 0.24$ (as did the earlier Tunes A and DW [18,19,21], but based on fewer data), which has been adopted as the new default value in Tune 1. Such a change leads to large differences in the extrapolation to LHC energies.

A second difference is the matter profile of the hadron. In the original model, a double Gaussian distribution was found to best reproduce the data, where a more "lumpy" proton gives rise to more fluctuations from the MPI framework. In [23], it is noted that the introduction of showers from MPI scattering systems gives rise to a new source of fluctuations such that it is possible to describe the same data with a single Gaussian matter distribution. It should be noted that this extra shower activity also ties in with the increase in $E_{\rm CM}^{\rm pow}$ above.

The differences between these tunes represents an uncertainty in our predictions. To give some indication of this uncertainty in what follows, certain data will be presented using both of these tunes, where, for simplicity, they will be referred to as the "old" and "new" tune respectively. Of course, these parameters are not changed in isolation and other parameters in the spacelike showers, MPI and beam remnants handling have been shifted

accordingly. More details on the current status of PYTHIA 8 tunes are available in the documentation contained within the package.

4 Rescattering

An event with a rescattering occurs when an outgoing state from one scattering is allowed to become the incoming state of another scattering. In the simplest case, one incoming parton to a scattering will be taken from the beam, while the other will come from a previous interaction (a single rescattering). There is, however, the possibility that both incoming partons will be already scattered partons (a double rescattering). If we accept MPI as real, then we should also allow rescatterings to take place. They would show up in the collective effects of MPI, manifesting themselves as changes to multiplicity, $p_\perp$ and other distributions. Unfortunately, these effects may not be so easy to detect in real life; some of the effects of rescattering will already be accounted for by the tuning of the existing models, e.g. slight parameter changes in ISR, FSR and the existing MPI framework. After implementing a model for rescattering, a retuning of $p_{\perp 0}$ and other parameters will be necessary so that rescattering contributions are not double counted. After such a retuning, it is likely that the impact of rescattering will be significantly reduced, so we should therefore ask whether there are more direct ways in which rescattering may show up. Is there perhaps a region of low $p_\perp$ jets, where an event is not dominated by ISR/FSR, where this extra source of three-jet topologies will be visible? A further consideration is that such rescatterings will generate more $p_\perp$ in the perturbative region, which may overall mean it is possible to reduce the amount of primordial $k_\perp$ and colour reconnections necessary to match data, as discussed in Sec. 3.3.

A comparison between double parton scattering and a single rescattering process is given in an analytical calculation by Paver and Treleani [26]. Specifically, they look at processes of the type illustrated in Fig. 1, which are both of the same order in α_s, but differ in the number of partons taken from the incoming hadrons. We will not cover this calculation in detail, but we make note of one interesting aspect. In the single rescattering case, the parton which goes on to rescatter is now a propagator, which introduces a $(1/p^2)$ term in the scattering amplitude. As usual, the approximation of taking the residue of the pole at $p^2 = 0$ can be made, but there is perhaps a slight contradiction when considering the space-time picture of two Lorentz contracted hadrons passing through each other. If the virtuality of the propagator gives some indication of the spatial separation of the two interactions, then one may expect some kind of characteristic scale given by the hadronic dimension, which is not taken into account in this approximation. Nevertheless, it is this same scheme which we will use as a starting point in our modeling of rescattering that follows. In this way, we can assume that a probabilistic description of rescattering can be used, as is already done for the existing MPI framework.

Some results of these analytical calculations are given in Sec. 5, but here we point out that this is a fully parton level calculation and does not include any radiative or hadronisation effects. The goal within the complete generation framework is not only to include all such effects, but also to model "higher-order" rescatterings in the same way that many MPI processes are included beyond DPS.

4.1 Rescattering and PDFs

To understand the basic principles of rescattering, we begin with the typical case of small-angle $2 \to 2$ scattering mediated by a t-channel gluon exchange. An incoming parton extracted from the hadron beam will still exist in the final state, only slightly disturbed in momentum space, and can still be associated with the same hadron beam. In the limit where the angle goes to zero, this parton has the same x value as the incoming one, previously selected according to the appropriate PDF. This parton thus contributes to the overall PDF of the beam with a delta function at the selected x (and with the given flavour), so that the new PDF can be written as

$$f(x, Q^2) \to f_{\text{rescaled}}(x, Q^2) + \delta(x - x_1) \tag{18}$$

where f_{rescaled} is the original PDF of the hadron, now rescaled to take into account the flavour and momentum taken from it, and x_1 is the x value of the extracted parton. In such a picture, the momentum sum should still be conserved

$$\int_0^1 x \left[f_{\text{rescaled}}(x, Q^2) + \delta(x - x_1) \right] \mathrm{d}x = 1 \ . \tag{19}$$

It can be viewed as a quantum mechanical measurement of the wave function of the incoming hadron, where the original squared wave function $f(x, Q^2)$ in part collapses by the measurement process of one of the partons in the hadron; that is, one degree of freedom has now been fixed, while the remaining ones are still undetermined. All the partons of this disturbed hadron can scatter, and so there is the possibility for the already extracted parton to scatter again.

We can generalise the above reasoning in two ways: first, to extract more than just one parton from the hadron and second, to move beyond only small angle gluon exchange, such that overall we may write the modified PDF as

$$f(x, Q^2) \to f_{\text{rescaled}}(x, Q^2) + \sum_i \delta(x - x_i) = f_{\text{u}}(x, Q^2) + f_{\delta}(x, Q^2) \ . \tag{20}$$

The sum over delta functions now runs over all partons that are available to rescatter, including outgoing states from hard/MPI processes and partons from ISR/FSR branchings, and the subscripts u/δ refer to the continuous "unscattered" and scattered components respectively.

When the full range of MPI processes and ISR/FSR branchings are allowed, it is no longer possible to associate each outgoing parton with a particular hadron remnant. This means that an appropriate prescription is required to associate partons with the beam remnants. This is addressed further below.

With the PDF written in this way, the original MPI probability given in eqs. (2) and (4) can now be generalised to include the effects of rescattering

$$\frac{\mathrm{d}\mathcal{P}_{\text{MPI}}}{\mathrm{d}p_\perp} \to \frac{\mathrm{d}\mathcal{P}_{\text{uu}}}{\mathrm{d}p_\perp} + \frac{\mathrm{d}\mathcal{P}_{\text{u}\delta}}{\mathrm{d}p_\perp} + \frac{\mathrm{d}\mathcal{P}_{\delta\text{u}}}{\mathrm{d}p_\perp} + \frac{\mathrm{d}\mathcal{P}_{\delta\delta}}{\mathrm{d}p_\perp}, \tag{21}$$

where the uu component now represents the original MPI probability, the uδ and δu components a single rescattering and the $\delta\delta$ component a double rescattering. In this way, rescattering interactions are included in the common $p_\perp$ evolution of MPI, ISR and FSR.

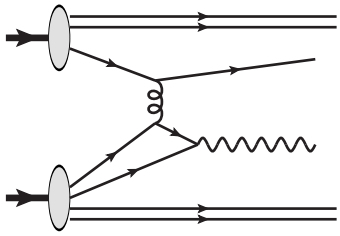

Figure 2: Z^0 production with a preceeding rescattering, which is not considered in our approach

This interleaving introduces a certain amount of coherence. For instance, it is possible for an outgoing parton from one interaction to branch, with one of the daughters rescattering, but such a branching must occur at a scale larger than that of the rescattering. There would not be time for a shower first to develop down to low scales, and thereafter let one of those daughter partons rescatter at a high scale.

We should remind that, as before, the $p_\perp$ ordering should not be viewed as a time ordering but rather as a resolution ordering. What this means is that, if viewed in a time-ordered sense, a parton could scatter at a high $p_\perp$ scale and rescatter at a lower one, or the other way around, with comparable probabilities. As will become apparent later on, the kinematics of scattering, rescattering and showers combined can become quite complex, however. Therefore we make one simplification in this article, in that we choose to handle kinematics as if the rescattering occurs both at a lower $p_\perp$ *and* a later time than the "original" scattering. The rescattering rate is not affected by this kinematics simplification.

This choice should not be a serious restriction for the study of jet and UE/MB physics, as is the main objective of this article. It does make a difference e.g. for Z^0 production combined with a rescattering. Assuming that the Z^0 vertex is at the largest scale and therefore defines the original scattering, it would not be allowed to have a rescattering that precedes the Z^0 production, i.e. the ordering illustrated in Fig. 2 would be excluded. Thus, for now, there is no natural way to study whether the rescattering mechanism could be used as a way to reduce primordial $k_\perp$ (Sec. 3.3).

4.2 Beam Association

We now return to the issue of associating scattered partons, that potentially may rescatter, with a beam remnant. A parton associated with beam A is allowed to rescatter with any of the partons from beam B, and vice versa. There are no first principles involved, except that the description should be symmetric with respect to beams A and B. We therefore consider four separate rapidity based prescriptions, some with tunable parameters $y_{\rm sep}$ and Δ_y. Expressed in the rest frame of the collision, with beam A (B) moving in the $+z$ ($-z$) direction, the probability for a parton to be assigned to beam A is

1. Simultaneous: each parton is treated as belonging to both incoming beams simultaneously
$$P_A = 1 \ .$$

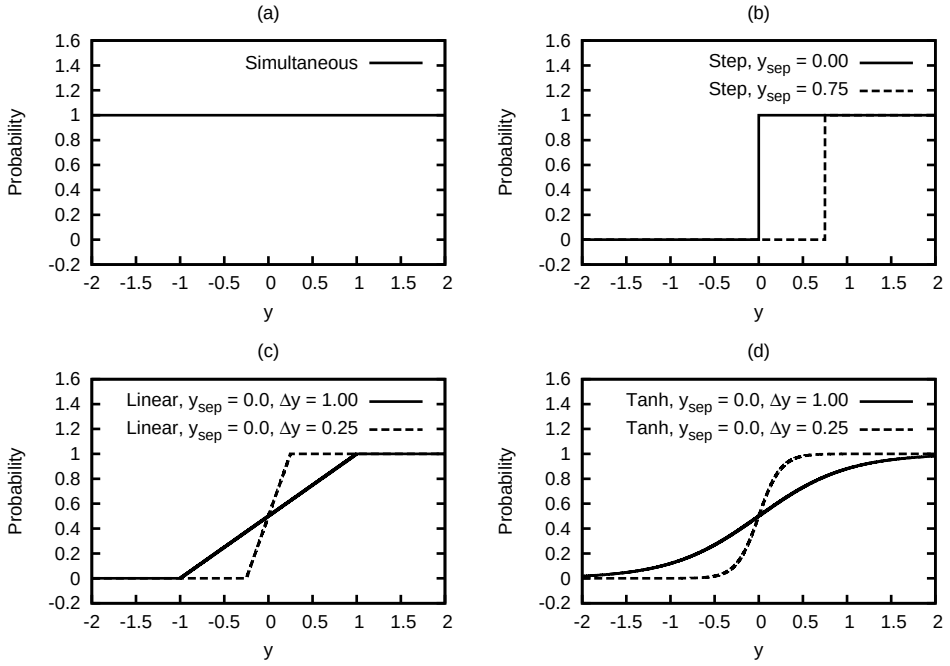

Figure 3: Probability of a parton being assigned to beam A for (a) Simultaneous (b) Step (c) Linear and (d) Tanh

2. Step: the probability for assignment to beam A is given by a step function in rapidity with an optional central exclusion or overlap region specified by $y_{\rm sep}$

$$P_A = \Theta(y - y_{\rm sep}) \ .$$

3. Linear: the probability for assignment to beam A is zero below $(y_{\rm sep} - \Delta_y)$, unity above $(y_{\rm sep} + \Delta_y)$ and rises linearly in between

$$P_A = \frac{1}{2}\left(1 + \frac{y - y_{\rm sep}}{\Delta_y}\right) \ , \quad y_{\rm sep} - \Delta_y < y < y_{\rm sep} + \Delta_y \ .$$

4. Tanh: the probability for assignment to beam A rises as

$$P_A = \frac{1}{2}\left(1 + \tanh\left(\frac{y - y_{\rm sep}}{\Delta_y}\right)\right) \ .$$

These four scenarios are illustrated in Fig. 3, which shows the probability of a parton being assigned to beam A for various parameter settings.

At first glance, it may appear that the simultaneous option will lead to many more rescatterings, as essentially twice the number of partons will be made available to rescatter compared to e.g. the step function with $y_{\rm sep} = 0$. Specifically, consider the single rescattering cross section for a given rescattering parton

$$\frac{{\rm d}\sigma}{{\rm d}p_\perp^2} = \sum_i \int {\rm d}x_1 \, f_i(x_1, Q^2) \, \frac{{\rm d}\hat{\sigma}}{{\rm d}p_\perp^2} \ . \tag{22}$$

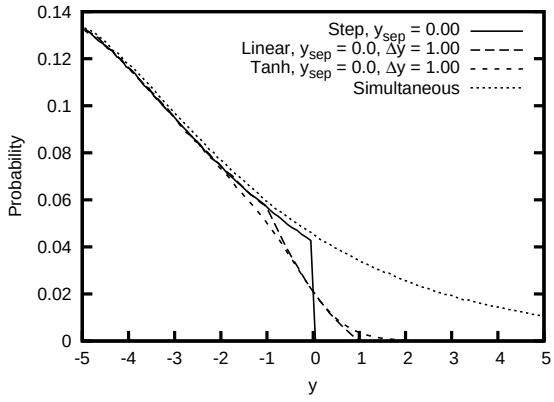

Figure 4: Probability of a parton being assigned to Beam B and being rescattered in LHC minimum bias events (pp, $\sqrt{s} = 14\,\text{TeV}$, old tune)

For t-channel gluon exchange, $\mathrm{d}\hat{\sigma}/\mathrm{d}p_\perp^2$ is almost independent of the mass of the colliding system. This requires, however, that the squared invariant mass fulfills $\hat{s} \geq p_\perp^2/4$, else obviously the cross section vanishes. The consequence is that the allowed x integration range will be smaller when the rescattering parton is in the same hemisphere as the yet to be selected parton, and larger when they are in opposite ones. The difference is quite marked in the small-x region, where the PDFs peak, resulting in only a modest increase in the single rescattering rate for the simultaneous option.

For double rescattering with the simultaneous option, a doubling of the number of interactions is immediately expected, relative to the step function, just from interchanging the partons assigned to beam A and beam B. A further (approximate) doubling of the number of pairs comes from considering also those with the two incoming partons in the same hemisphere. At first glance, one might guess that these latter ones again would be suppressed by the mass requirement. However, note that this time there is no integration down to small x involved, since the incoming parton momenta are already fixed. Furthermore, since the evolution is done in order of decreasing $p_\perp$, the incoming partons were both produced at a larger $p_\perp$ scale than is now considered for the rescattering. Therefore, already the separation in the transverse momentum plane is typically enough to fulfill the $\hat{s}$ condition, even without the further separation of longitudinal momenta.

Finally, the linear and tanh options can be seen as smeared-out versions of the step one, where one could argue the tanh option as being more physical since it contains no discontinuities.

To get an idea of the effects of the various options, we study some features of LHC minimum-bias events (pp, $\sqrt{s} = 14.0\,\text{TeV}$, old tune) when no showers are present. Fig. 4, shows the probability for a parton to be assigned to beam B and subsequently to be rescattered as a function of rapidity. The natural suppression in the simultaneous scenario, as discussed above, is visible in the positive rapidity region. Fig. 5 now shows the $p_\perp$ distributions of (a) single rescatterings and (b) double rescatterings. With the simultaneous option the increase in single rescatterings is small, as expected. It is the factor four rise in double rescattering that now stands out; as explained above there is almost no suppression in interactions where the two partons sit in the same hemisphere.

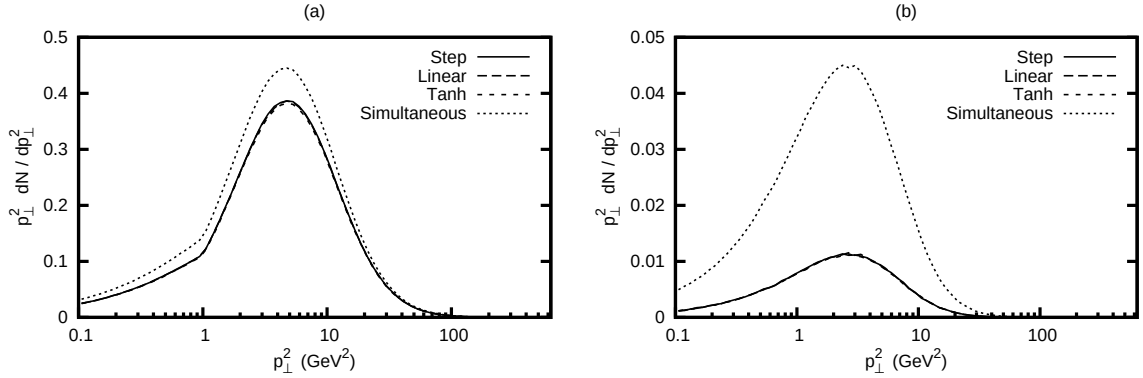

Figure 5: $p_\perp$ distributions of (a) single rescatterings and (b) double rescatterings in LHC minimum bias events (pp, $\sqrt{s} = 14\,\text{TeV}$, old tune). Parameters for the different options are the same as the previous figure. Note the difference in vertical scale between (a) and (b), and that the step, linear and tanh curves are so close that they may be difficult to distinguish

At this stage, it is clear that the different beam prescriptions do not have a large influence on the outcome of rescattering, except for double rescattering when used with the simultaneous option. In Fig. 6a, the $p_\perp$ distributions of normal MPI scatterings are shown compared to those of single rescattering for both the old and new Pythia 8 tunes. The effect of the different tunes on the extrapolation of the MPI model to LHC energies is immediately apparent. As previously predicted, rescattering is a small effect at larger $p_\perp$ scales, but, when evolving downwards, its relative importance grows as more and more partons are scattered out of the incoming hadrons and become available to rescatter. The suppression of the cross section at small $p_\perp^2$ is caused mainly by the regularisation outlined in eq. (5), but is also affected by the scaling violation in the PDFs. Below $p_\perp^2 \sim 1\,\text{GeV}^2$ the PDFs are frozen, giving rise to an abrupt change in slope. Normal scatterings dominate, but there is a clear contribution from single rescatterings. Double rescattering is too small to be visible in the upper plot, but included in the lower plot is the ratio of double rescattering to normal rescattering for the simultaneous option, where the old tune has been used to generate the maximum effect possible. Even in this maximal case, the growth of double rescattering with lowering $p_\perp$ is slow, peaking around the 10% level in the low-$p_\perp$ region where it is likely that any effects will be "washed out" by other low $p_\perp$ activity.

Although, in this formalism, rescattering is a low-$p_\perp$ effect (insofar as it occurs at low scales in the $p_\perp$ evolution of the event), we point out that it can have an effect on the high-$p_\perp$ properties of an event. Fig. 6b shows the probability for a parton created in the hard process of an event to go on and rescatter as a function of the initial $p_\perp$ of the parton. A parton created at a high $p_\perp$ will have a larger range of $p_\perp$ evolution, meaning that there is a greater chance that it will rescatter at some point in this evolution.

Finally, as an indicator of the effect of energy on the growth of rescattering, Table 1 shows the average number of scatterings and rescatterings for different types of event at Tevatron and LHC energies (step option only, old and new tunes). With all these points in mind, from now on we no longer consider double rescattering effects and restrict ourselves to the step beam prescription; with just these options, the implementation is simplified

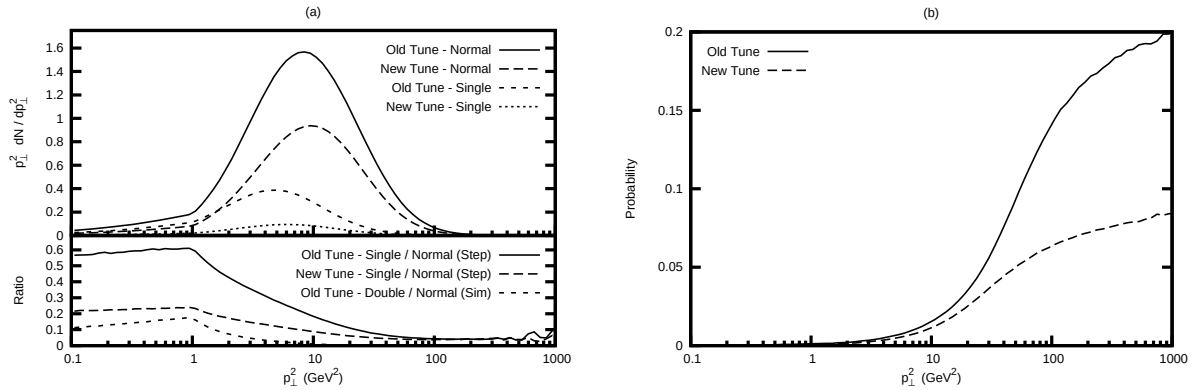

Figure 6: Rescattering in LHC minimum bias events (pp, $\sqrt{s} = 14\,\text{TeV}$, old and new tunes). (a) shows the $p_\perp$ distribution of scatterings and single rescatterings per event. Included in the ratio plot is double rescattering with the simultaneous beam prescription using the old tune, where its effect is maximal. (b) shows the probability for a parton, created in the hard process of an event, to rescatter as a function of its initial $p_\perp$

		Tevatron		LHC	
		Min Bias	**QCD Jets**	**Min Bias**	**QCD Jets**
Old	**Scatterings**	2.81	5.09	5.19	12.19
	Single rescatterings	0.41	1.32	1.03	4.10
	Double rescatterings	0.01	0.04	0.03	0.15
New	**Scatterings**	2.50	3.79	3.40	5.68
	Single rescatterings	0.24	0.60	0.25	0.66
	Double rescatterings	0.00	0.01	0.00	0.01

Table 1: Average number of scatterings, single rescatterings and double rescatterings in minimum bias and QCD jet events at Tevatron ($p\overline{p}$, $\sqrt{s} = 1.96\,\text{TeV}$, QCD jet $\hat{p}_{\perp\text{min}} = 20\,\text{GeV}$) and LHC (pp, $\sqrt{s} = 14.0\,\text{TeV}$, QCD jet $\hat{p}_{\perp\text{min}} = 50\,\text{GeV}$) energies for both the old and new tunes

while the bulk of the interesting phase space region is still covered.

4.3 Inclusion of Radiation and Beam Remnants

The addition of rescattering has non-trivial effects on the colour flow in events. Without rescattering, in the $N_C \to \infty$ limit, all colours are confined within a $2 \to 2$ scattering subsystem. With rescattering, you now have the possibility for colour to flow from one system to another, and thereby to form radiating dipoles stretched between two systems. Should we then expect differences in radiation, relative to a normal dipole confined inside a subsystem? A crude qualitative argument is that, for a rescattering dipole, there are more propagators sitting between radiator and recoiler than normally, which, in an average sense, corresponds to a larger spatial separation. As a result, one may expect a suppression of hard radiation, with the normal full rate only in the soft limit.

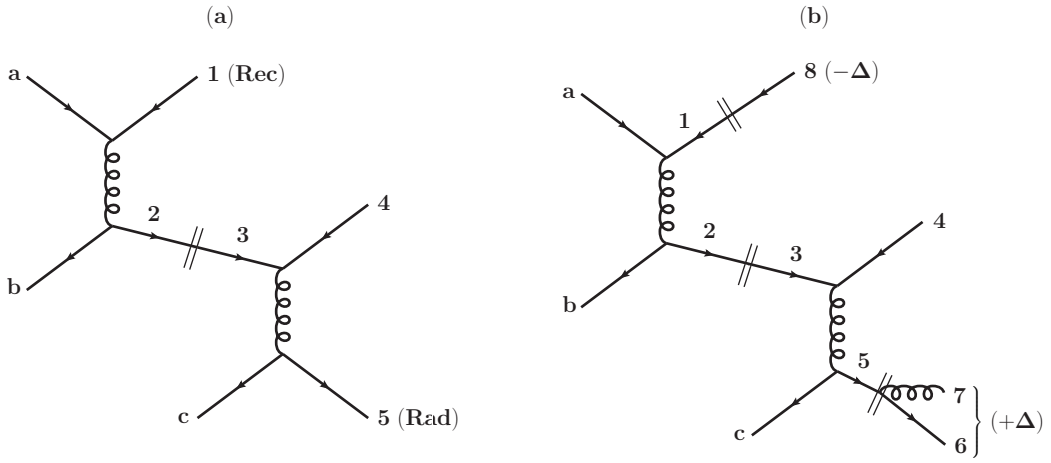

Figure 7: Final-state dipole spanning two scattering subsystems (a) before branching and (b) after branching. Δ is the four-momentum transferred from the recoiler to the radiator and the double lines indicate where a new particle has been bookkept

This is not the only new issue when showers and beam remnants are to be combined with the rescattering concept. There are considerable technical complications when we consider those steps of event generation that rely on Lorentz boosts to kinematically shift partons, specifically ISR and primordial $k_\perp$. For instance, consider a situation where a final-state dipole spans two systems, such as in Fig. 7. In (a), partons 1 and 2 are outgoing from the first system, parton 3 is the rescattering parton now incoming to the second system (identical to parton 2, but marked separately for clarity) and partons 4 and 5 are outgoing from the second system. We now consider what happens when parton 5 radiates a gluon with parton 1 as its recoiling partner. In the existing framework, the situation after the branching is shown in (b); parton 5 has branched into partons 6 and 7, while parton 8 now reflects the changed kinematics of the recoiler. After the branching, both systems combined still conserve energy and momentum, but individually they do not.

Alone, this is not a significant issue. However, the introduction of initial-state branchings and primordial $k_\perp$ means that the incoming partons a, b and c time and again receive a changed four-momentum. More specifically, it is this $p_\perp$ kick combined with longitudinal momentum and energy transfer that guarantees that the invariant mass of the $a + b$ and $c + 3$ systems are preserved. However, while $p_c + p_3 = p_4 + p_5$, such that any $p_\perp$ kick on c is transferred to the $4 + 5$ final state, after the dipole emission $p_c + p_3 \neq p_4 + p_6 + p_7$. Thereby the kick on the final state will become wrong, leading to an overall imbalance in an event. The effect is especially big if the original lightcone momentum of c is very small, while that of 1, along the same axis, is large. Then a modest transfer from 1 to $6 + 7$ can give a big multiplication factor for a $p_\perp$ kick on c.

The solution we have adopted is, for FSR, to propagate momentum shifts through all intermediate systems, such that energy and momentum are conserved locally in all systems. Fig. 8 shows how the branching of Fig. 7 now looks with this scheme. It is now partons 8 and 9 that are outgoing from the first system, while it is parton 10 and no longer parton 3 that is incoming to the second system.

The example shown is one of the simplest possible; there can be one or more intermediate

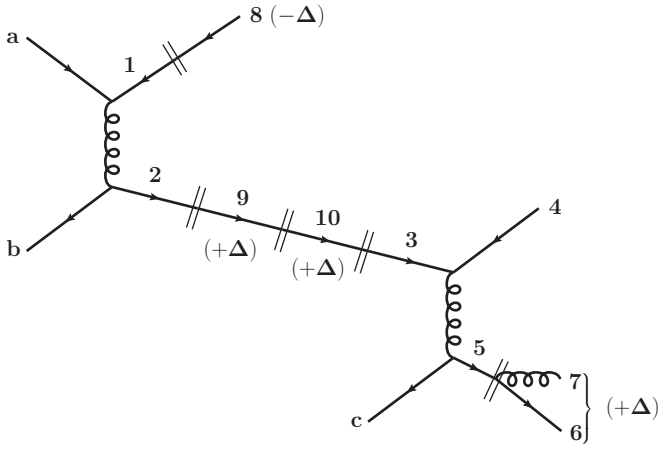

Figure 8: Branching of a final-state dipole spanning two scattering subsystems where the internal line connecting the two systems has been changed to conserve momentum

systems sitting between the radiating and recoiling systems, such that it is more than one intermediate line that must have its momentum changed. It is also important to note that the momentum transfer has already been defined by the procedure of keeping the dipole mass unchanged. This means that, when propagating the recoil along all internal lines connecting the systems, the partons are going to acquire nonzero virtualities, spacelike or timelike.

This scheme does allow for the complete parton shower and hadronisation framework to be used, but does have disadvantages. Firstly, this procedure is only valid when a path can be found that connects the radiating and recoiling systems, which for QCD radiation will almost always be true. When there is no direct path between the two different systems, the emission is vetoed. In principle this procedure may then be carried out for all branchings that meet the above criteria, but in practice we identify the following cases where additional vetoes are required:

- Negative system $\hat{s}$: this scheme can result in both the invariant masses and rapidities of systems being altered. While we explicitly allow this to happen, there is the restriction that the $\hat{s}$ of a system may not turn negative. Any branching that would cause such a situation is therefore vetoed.
- Too large virtuality or negative energy: Lorentz transformations mix the energy and momentum components of a four-vector. Allowing the virtuality of an incoming or outgoing parton to become large in comparison to the invariant mass of its system, or allowing an outgoing parton to have an arbitrarily large negative energy would result in partons gaining a large "unphysical" $p_\perp$ kick from a boost. This kick is compensated, so that momentum is conserved, but the transverse energy of the event may increase more than it should. Unfortunately, there are no simple criteria for deciding when a boost becomes too large such that it is deemed improper. The limits used are therefore to veto emissions when they cause a parton virtuality or energy (in the rest frame) to come within a certain fraction of the system invariant mass.

The suppression of FSR caused by this scheme is shown in Fig. 9 for LHC jet events (pp, $\sqrt{s} = 14.0\,\text{TeV}$, $\hat{p}_{\perp\text{min}} = 100\,\text{GeV}$, old tune). The upper plot shows the ratio of $p_\perp^2$ values

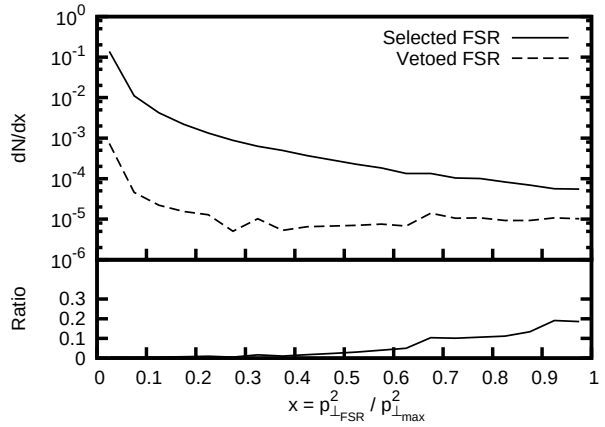

Figure 9: Amount of FSR vetoed by momentum propagation procedure (see text). LHC jet events (pp, $\sqrt{s} = 14\,\mathrm{TeV}$, $\hat{p}_{\perp\mathrm{min}} = 100\,\mathrm{GeV}$, $40 \leq p_{\perp\mathrm{max}} \leq 50\,\mathrm{GeV}$, old tune)

for final-state radiation to the maximal $p_\perp^2$ value (i.e. the creation scale of the system), for all selected $p_\perp^2$ values and for those that are then subsequently vetoed as above. Only radiation from rescattering systems produced with $40 \leq p_\perp \leq 50\,\mathrm{GeV}$ is considered for clarity. From the ratio plot, it is evident that the amount of radiation being vetoed per system is not large, reaching around 20% in the high-$p_\perp$ region, and that the pattern also follows what may be expected by the reasoning given above for FSR suppression; a perhaps not-unfortunate side effect of the vetoing procedure. Even with this suppression in place, there are still effects on those stages of the simulation that use Lorentz boosts. We return to these after first giving some details on ISR and primordial $k_\perp$.

To study ISR, again consider the situation in Fig. 7a. One case is when one of the incoming partons to a system is from the beam, and therefore can radiate within the usual backwards evolution picture, while the other is a rescattering parton, such as $c + 3$. As discussed in Sec. 3.2, these two incoming partons define an effective dipole. An initial-state emission will change the momentum of c. This situation can be handled in much the same way as in a normal $2 \to 2$ system, with the difference that parton 3 may have nonzero $p_\perp$ and may also have a mass so that the kinematics is more complicated [40].

Extra work is required when the radiating system has outgoing partons that go on to rescatter, however. That is, if either a or b obtain changed momentum by ISR, then also 1 and 2 are changed, and hence the incoming 3 of the rescattering system, and finally also the outgoing partons 4 and 5. There is then a choice to be made: to change the momentum of the other incoming parton c or not. In the latter case, with one incoming parton changed and the other not, the internal kinematics of the $3+c \to 4+5$ collision cannot be preserved. That is, its invariant mass and collision $p_\perp$ are changed, both of which we would rather preserve. Instead,to keep the system mass unchanged, the 4-momentum of the incoming parton c must be rescaled, up or down. In the case that the outgoing partons 4 and 5 go on to rescatter this procedure must be applied again to the new systems, until all daughter systems have had their kinematics updated. There is a price to pay in this approach, since any extra energy must be taken from one of the incoming beams. In the worst case, the extra energy may exceed what is available in the beam remnant. When this happens, the original hard process is kept, but the shower and MPI stages of the simulation are restarted.

To generate full events, the machinery of primordial $k_\perp$ must also be added. With the scheme outlined above, the boosts used here do not present any additional issues compared with the ISR boosts above. Only partons originating from the beams are given primordial $k_\perp$, and again, any $p_\perp$ kick given to a parton that goes on to rescatter will be propagated to all daughter systems. There is one further point to address, however. As explained in Sec. 3.3, the lightcone momenta of the two initiator partons to a system are rescaled to keep the invariant mass and rapidity of the system unchanged. If one of the incoming partons is now a rescattering parton, then it is natural to require its four-momentum to remain unchanged. If we do this, there are no longer enough degrees of freedom to keep both $\hat{s}$ and y of the system unchanged. The default choice, therefore, is to keep $\hat{s}$ unchanged, by a suitable scaling of the momentum of the incoming beam particle, but to allow the rapidity of the system to change. It may, however, be undesirable to allow the rapidities of systems to change, so there is an additional option to allow the lightcone momentum of the rescattering parton to change, such that both $\hat{s}$ and y can be maintained.

Finally, we study the potential effects of the above scheme on events. With rescattering, we expect some deviation from the "standard" case for how Lorentz boosts of ISR and primordial $k_\perp$ affect events; the question is how we can quantify these deviations. As a metric, for each system undergoing a boost, we use two quantities, $p_{\perp\text{kick}}$ as a measure of the expected $p_\perp$ shift of a system and $p_{\perp\Delta}$ as a measure of the actual $p_\perp$ shift of a system, defined as

$$p_{\perp\text{kick}} = (p_1' + p_2' - p_1 - p_2)_\perp \ , \tag{23}$$

$$p_{\perp\Delta} = \sum_{\substack{\text{outgoing}\\\text{after}}} p_\perp - \sum_{\substack{\text{outgoing}\\\text{before}}} p_\perp \ . \tag{24}$$

Here, p_1, p_2 are the previous incoming four-vectors to a system, p_1', p_2' are the new incoming four-vectors to a system and the sums are over all outgoing partons of a system, after and before the boost has been performed. Interpreting these measures is not completely straightforward. For instance, if we consider two back-to-back jets with transverse momenta only in the p_y direction, then a boost purely in the p_x direction will result in a $p_{\perp\Delta} < p_{\perp\text{kick}}$. Indeed, most of the boosts will have such a configuration, but a per-event quantity

$$p_{\perp\text{diff}} = \frac{\sum_{\text{systems}} \max\left(0, p_{\perp\Delta} - p_{\perp\text{kick}}\right)}{\sum_{\text{final}} p_\perp} \ , \tag{25}$$

where the first sum is over all systems that are boosted in either ISR or primordial $k_\perp$, and the second sum over all final state particles, can be used to give an indication of those events where we may be giving extra unwanted $p_\perp$ to certain systems, which is where the biggest concern lies. The results of this are shown in Fig. 10 for LHC QCD jet events (pp, $\sqrt{s} = 14\,\text{TeV}$, $\hat{p}_{\perp\text{min}} = 100\,\text{GeV}$, old tune), split into contributions from ISR and primordial $k_\perp$. An immediate observation is that, without rescattering, ISR does not give any tail according to this measure, while primordial $k_\perp$ does. Here, it is important to note that the procedure of shifting the frame of a system will often involve rotations which can skew the $p_\perp$ of a system and it is the boosts of primordial $k_\perp$, where both incoming partons to a

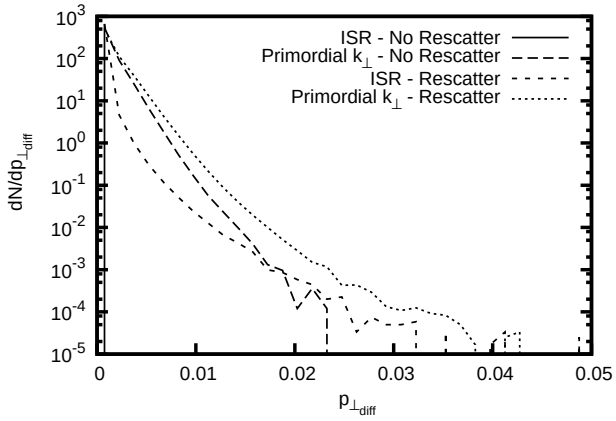

Figure 10: Effects of the modified ISR/FSR/MPI scheme on those stages involving Lorentz boosts. LHC jet events (pp, $\sqrt{s} = 14\,\text{TeV}$, $\hat{p}_{\perp\text{min}} = 100\,\text{GeV}$, old tune). $p_{\perp\text{diff}}$ is defined in eq. (25)

system are simultaneously changed, which are the most extreme. The effects of primordial $k_\perp$ are increased when rescattering is introduced, and also ISR enters the game, but it is important to note that there is no qualitative change of the shape. Overall, we find that in around 1 event in 100,000 there is an extra $p_\perp$ of around 1% of the total event $p_\perp$, which, although not ideal, is not too worrying.

5 Results

5.1 Parton Level

We begin by returning to the analytical calculation of Paver and Treleani [26]. To get an idea of the relative number of events for DPS and single rescattering, they integrate their cross sections from a transverse energy of 40 GeV upwards over a rapidity interval of $|y| < 1$ for each jet. For both the three-jet and four-jet cross sections, they look at two cases: one where all jets must have $E_\perp > 10\,\text{GeV}$ and another where one of the jets is allowed to have $E_\perp > 5\,\text{GeV}$, while the rest must have $E_\perp > 10\,\text{GeV}$. Their results for Tevatron energies ($\text{p}\overline{\text{p}}$, $\sqrt{s} = 2\,\text{TeV}$) are shown in Fig. 11a as a function of the summed transverse energy of the jets, with the two-jet cross section given for comparison. In each case, the three-jet cross section is smaller than its four-jet counterpart, but still suggests that rescattering may be a noticeable source of three-jet topologies.

We now move on to the results from Pythia, where the same cuts as in Fig. 11a have been used. We also begin with Tevatron energies ($\text{p}\overline{\text{p}}$, $\sqrt{s} = 2\,\text{TeV}$) using the old PDF parameterisation of Glück, Hoffmann and Reya (GHR) [45] as in the analytical calculation. Both the hard process and multiparton interaction processes in Pythia are limited to light QCD (u, d, s) only, but the full 1st order running of α_s has been left in place, however. Qualitatively, the results from Pythia are similar to the analytical calculation.

One interesting difference is the larger three-jet cross section (compared to four jets) when all jets have $E_\perp > 10\,\text{GeV}$ at high $E_\perp$ values. The key difference between DPS and

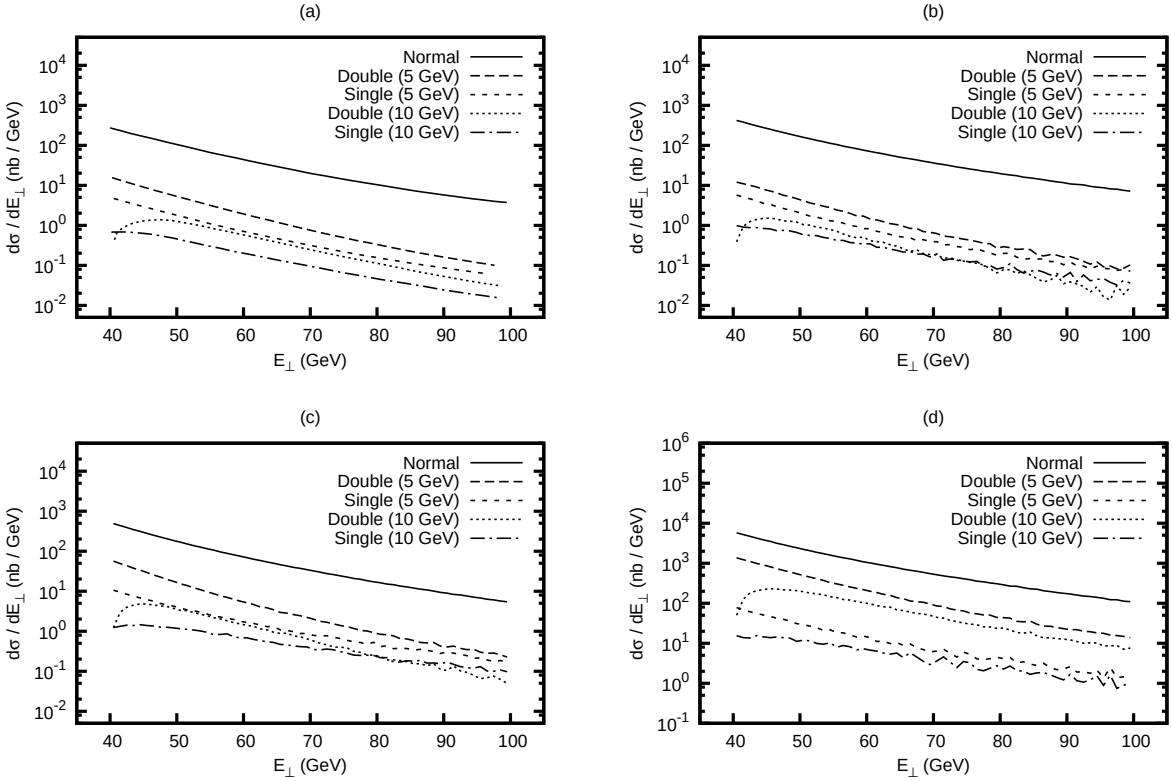

Figure 11: Parton level jet cross sections with $|y| < 1.0$. Normal, single and double refer to the two-, three- and four-jet cross sections respectively. "10 GeV" refers to the case where all jets must have $E_\perp > 10\,\text{GeV}$ while "5 GeV" refers to the case where one jet must have $E_\perp > 5\,\text{GeV}$ and the remaining ones must have $E_\perp > 10\,\text{GeV}$. Plots show (a) analytical results of Paver and Treleani, $\text{p}\overline{\text{p}}$, $\sqrt{s} = 2.0\,\text{TeV}$; (b) PYTHIA, $\text{p}\overline{\text{p}}$, $\sqrt{s} = 2.0\,\text{TeV}$, GHR PDF parameterisation, light QCD only, new tune; (c) PYTHIA, $\text{p}\overline{\text{p}}$, $\sqrt{s} = 2.0\,\text{TeV}$, CTEQ5L PDF, all heavy quark effects, new tune; (d) PYTHIA, pp, $\sqrt{s} = 14.0\,\text{TeV}$, CTEQ5L PDF, all heavy quark effects, new tune

single rescattering events are the number of partons taken from the incoming hadrons; four in the former and three in the latter. Assuming that the hardest $2 \to 2$ process has taken place, we are left with the PDF integrals given in eq. (1) for DPS and eq. (22) for single rescattering. Given the $E_\perp$ scales in question, one would naïevly expect the PDF weights for rescattering to be smaller than those for DPS, but now we must consider the effects of the rapidity cut, $|y| < 1$. With DPS, for both jets to lie within this central rapidity region, the x integration ranges of the two PDFs are now linked such that a large x value from one PDF factor must be matched by a similarly large x value from the other. In this way, the four-jet cross section falls off faster than the three-jet one as we start to consider harder jets in the central rapidity region. Taken to the extreme, for MPI jets in a very narrow bin in rapidity, we would expect the four-jet cross section to be suppressed.

We now stay with Tevatron events, but move on to the newer CTEQ5L PDF set, as well as allowing all possible QCD hard processes and the full set of default MPI processes. Heavy quark effects are expected to be small, so most changes will be driven by differences in the PDFs. A key difference between the two sets is the gluon content; CTEQ5L has a

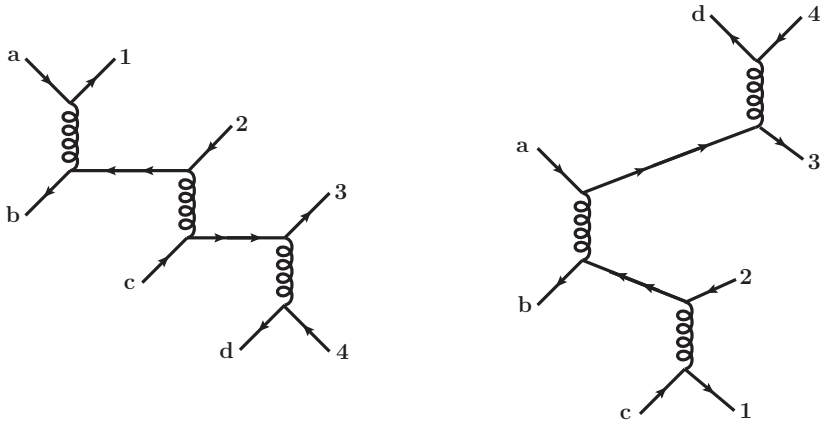

Figure 12: Two examples of $4 \to 4$ topologies which come from two single rescatterings. The $p_\perp$ scale of each interaction decreases moving from left to right and each diagram has four incoming (a, b, c, d) and four outgoing (1, 2, 3, 4) partons

softer distribution, making it easier to extract low-x gluons in the kinematically relevant region. The results are shown in Fig. 11c. As expected, both the three- and four-jet cross sections are higher. The ratio of four- to three-jet cross sections also has increased slightly, especially at low-$E_\perp$, reflecting that the increased gluon number in both beams makes DPS more favourable. Finally, in Fig. 11d, the results are shown for LHC energies (pp, $\sqrt{s} = 14\,\text{TeV}$, new tune). Both four-jet cross sections now sit well above their three-jet counterparts and the reasoning as for Fig. 11c still holds; the increase in the PDFs of both beams makes DPS more likely. The results for the old tune are not shown, but show essentially the same picture; the extra MPI activity leads only to a slight increase in the three- and four-jet cross sections.

Unfortunately, this is not the end of the story. Both the three- and four-jet cross sections have large radiative contributions, and it is to these that we must compare rescattering. To do this we now run with the full ISR, FSR and MPI frameworks (but remain at the parton level), and look at the makeup of the different cross sections. Here we look at events after the first few steps in the downwards $p_\perp$ evolution only; although there will still be contributions to the cross-sections from later stages in the evolution, we only aim to capture the dominant contributions in the following. For the three-jet case, we identify the following contributions: (a) $2 \to 3$ from single radiation, (b) $3 \to 3$ from a single rescattering, and (c) $4 \to 3$ from DPS with one jet lost due to cuts. Instead, for the the four-jet case, we identify: (a) $2 \to 4$ from double radiation, (b) $3 \to 4$ from single radiation + a single rescattering, (c) $4 \to 4$ from DPS, and (d) $4 \to 4'$ from two single rescatterings (e.g. Fig. 12). The different contributions, as a function of the summed $p_\perp$ of the jets, are shown in Fig. 13 for LHC minimum bias events (pp, $\sqrt{s} = 14\,\text{TeV}$, new tune) when no rapidity or $p_\perp$ cuts are applied. Without a rapidity cut, the $4 \to 3$ configuration is now not possible. The radiative contributions are dominant over most of the $p_\perp$ range, but there is a low-$p_\perp$ region where the DPS cross section is also large. The $3 \to 3$ and $3 \to 4$ rescattering contributions are suppressed by roughly two orders of magnitude. Finally, we note that there is a contribution, albeit small, from 2 single rescatterings leading to a $4 \to 4'$ configuration.

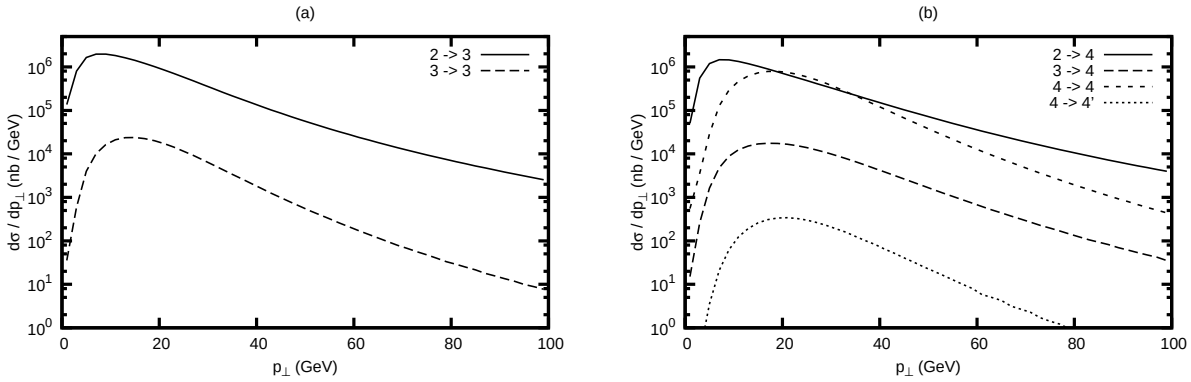

Figure 13: Breakdown of contributions to the (a) three-jet and (b) four-jet cross sections (see text) for LHC minimum bias events (pp, $\sqrt{s} = 14\,\text{TeV}$, new tune) when no $p_\perp$ or rapidity cuts are applied

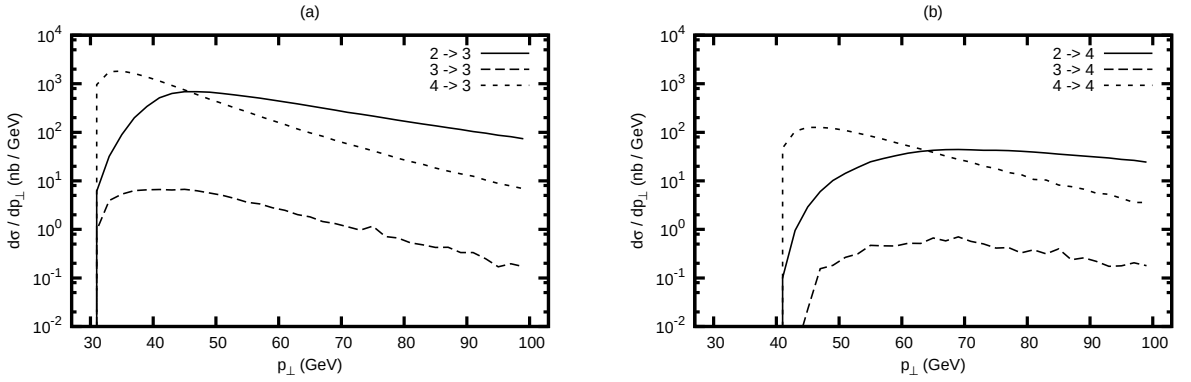

Figure 14: Breakdown of contributions to the (a) three-jet and (b) four-jet cross sections (see text) for LHC minimum bias events (pp, $\sqrt{s} = 14\,\text{TeV}$, new tune) with $p_\perp > 10\,\text{GeV}$ and $|\eta| < 1.0$

We now additionally introduce cuts, such that all jets must have a minimum $p_\perp$ and lie in some pseudorapidity range. One of the key effects of a pseudorapidity cut is the addition of a new source of 3-jet events; those coming from DPS, but where one of the jets does not fall within the allowed η range. The results for $p_\perp > 10\,\text{GeV}$ and $|\eta| < 1.0$ are shown in Fig. 14. Immediately it is obvious that those events where rescattering is present is small compared to the large background of radiative and DPS events. We also note that the $4 \to 4'$ sample is now too small to be visible in Fig. 14b.

The results so far are not too encouraging. The background to single rescattering is large, but we now move on to hadronic observables; here we can instead look for signs of the collective effects of the potentially many rescatterings per event. Further, in Sec. 5.4 we look to see if there are any kinematical differences which may distinguish events which contain rescattering.

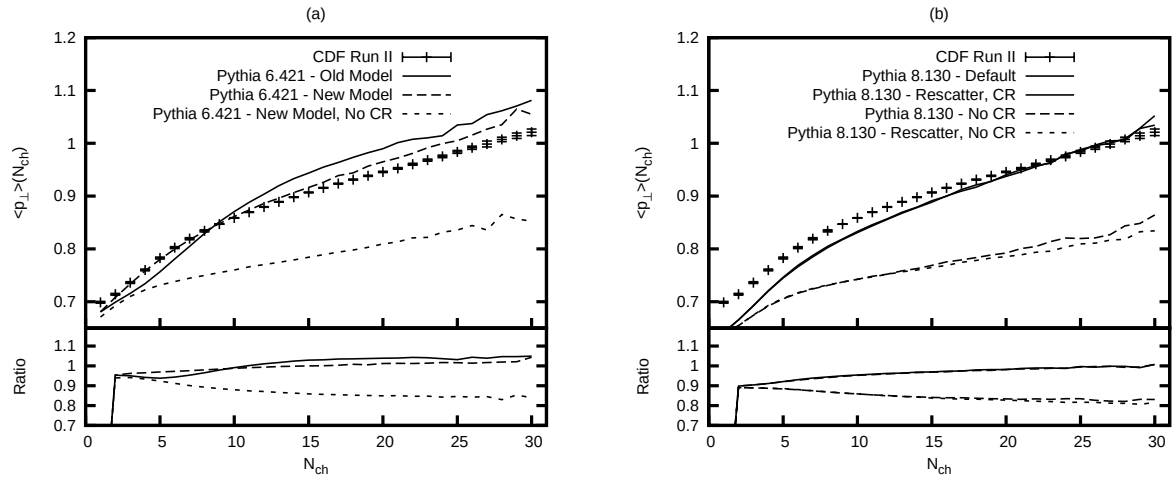

Figure 15: Mean $p_\perp$ as a function of charged multiplicity ($\mathrm{p\overline{p}}$, $\sqrt{s} = 1.96\,\mathrm{TeV}$, $p_\perp \geq 0.4\,\mathrm{GeV}$, $|\eta| \leq 1$). CDF Run II data is compared to (a) Pythia 6, old and new MPI models and (b) Pythia 8, new tune, now with rescattering included. With Pythia 8, the curves with colour reconnection, with and without rescattering, lie on top of each other

5.2 Colour Reconnection

We next turn our attention to colour reconnection. The key observable is the mean $p_\perp$ as a function of the charged multiplicity. Fig. 15a shows the CDF Run II data [46] and the results from the Pythia 6 generator. Events are generated using the soft QCD option and all charged particles with $p_\perp \geq 0.4\,\mathrm{GeV}$ and $|\eta| \leq 1$ are included, as in the experimental data. With only soft QCD allowed, the low multiplicity bins may miss some activity, e.g. from double diffractive events, but it is the higher multiplicities that concern us here. Both the old (Tune A) and new (Professor "Pro-pT0" tune) MPI models in Pythia 6 are shown and both do well in describing the data. Also shown is the new model with colour reconnection switched off. Turning reconnection off will result in an increase in multiplicity, so the procedure used here is to retune the $p_{\perp 0}$ parameter of the MPI framework such that the average charged multiplicity (using the same cuts as above) is the same as when colour reconnections are switched on. This is a crude retuning method, but serves well enough to show the desired effects. Without reconnection, and with a retuned $p_{\perp 0}$, it is clear that the rise in mean $p_\perp$ with multiplicity is much slower and does not come close to reproducing the data.

Fig. 15b shows the results for Pythia 8 (new tune), this time also with the addition of rescattering. Again, a tuning is performed such that the average charged multiplicity in each case is the same as the default curve (some indicative $p_{\perp 0}$ values, also for LHC energies, are given in the following section). The results, although not completely unexpected, are disappointing. The lack of change when rescattering is switched on means that the ratio of extra $p_\perp$ to multiplicity is essentially unchanged.

As it stands, rescattering does not contribute anything towards reducing the amount of colour reconnections required to match data. One point worth considering, however, is that the colour reconnection algorithm, as described in Sec. 3.3, has been essentially left unchanged with the addition of rescattering. One could ask e.g. if there are aspects of rescattering systems which means they should be reconnected in a different way? As such

			Old Tune		New Tune	
		$\sqrt{s}$ (TeV)	$p_{\perp 0}^{ref}$	$p_{\perp 0}$	$p_{\perp 0}^{ref}$	$p_{\perp 0}$
Original	**Tevatron**	1.96	2.15	2.18	2.25	2.30
	LHC	7.00	2.15	2.67	2.25	3.12
	LHC	14.0	2.15	2.99	2.25	3.68
Retuned	**Tevatron**	1.96	2.25	2.28	2.34	2.39
	LHC	7.00	2.28	2.83	2.34	3.23
	LHC	14.0	2.29	3.18	2.34	3.82

Table 2: $p_{\perp 0}$ values before and after tuning for Tevatron and LHC energies with the old and new tunes. The relation between $p_{\perp 0}^{\rm ref}$ and $p_{\perp 0}$ is given in eq. (6). $E_{\rm CM}^{\rm ref} = 1800\,{\rm GeV}$ for both tunes, while $E_{\rm CM}^{\rm pow} = 0.16$ for the old tune and $E_{\rm CM}^{\rm pow} = 0.24$ for the new

a study could potentially fill another article, we ignore such questions here, and note that the current procedure is correct, insofar as colour reconnection is a somewhat "ad-hoc" procedure.

5.3 Cronin Effect

As discussed in Sec. 2, the Cronin effect is the observation of an enhancement in high-$p_\perp$ particle production, relative to low-$p_\perp$ production, in proton-nucleus collisions compared to proton-nucleon (after some model-dependent scaling by a nuclear modification factor). It is postulated that some kind of rescattering contributes to this effect, so our goal is to see if we can observe any similar type of effect in pp/p$\overline{\rm p}$ interactions within our model. Although we are looking at high-$p_\perp$ hadron production, the underlying cause within the model is the (repeated) rescattering of existing partons out to higher overall $p_\perp$, even when each rescattering is likely to be rather soft.

The $p_\perp$-spectra of charged hadrons and neutral pions are taken in the range $|\eta| < 1.0$ with $p_\perp > 0.4\,{\rm GeV}$ using the minimum bias soft QCD option of Pythia. As before, a retuning of the $p_{\perp 0}$ parameter of MPI is performed when rescattering is switched on such that the average charged multiplicity, using the same cuts as above, is maintained. To give an idea of the order of magnitude of the changes required to $p_{\perp 0}$, the original and retuned values are given in Table 2 for the different energies and tunes used in this study.

We begin at the parton level; for an increased hadron production at high $p_\perp$, we expect the parton-level $p_\perp$ distribution to also be harder. To observe this, we study the parton level inclusive jet distribution (with ISR, FSR and MPI enabled), where partons must meet the same cuts described previously. Fig. 16 shows the ratio of the distributions with rescattering switched on (both untuned and tuned) to the default curve for LHC minimum bias events (pp, $\sqrt{s} = 14\,{\rm TeV}$, old and new tunes). When rescattering is switched on, but no retuning is performed, there is an overall rise in jet multiplicity across the entire $p_\perp$ range, although mostly at low $p_\perp$, as expected. The retuning is now performed (using the $p_{\perp 0}$ values from the hadron level tuning as described above), such that the excess multiplicity is now removed.

For the new tune, the retuned curve now sits below the default one over most of the $p_\perp$

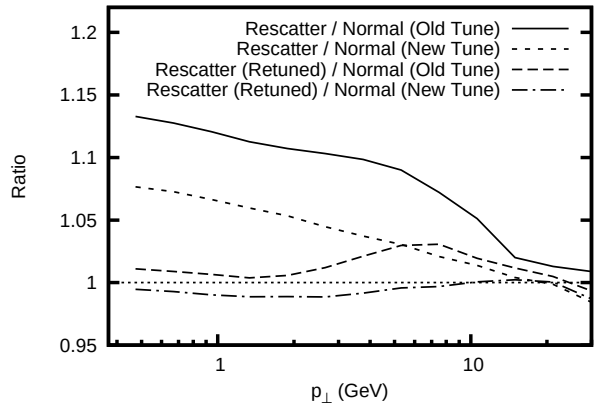

Figure 16: Ratios of rescattering (both tuned and untuned) to no rescattering for parton level inclusive jet distributions, LHC minimum bias events (pp, $\sqrt{s} = 14\text{TeV}$, $p_\perp > 0.4\text{GeV}$, $|\eta| < 1.0$, old and new tunes)

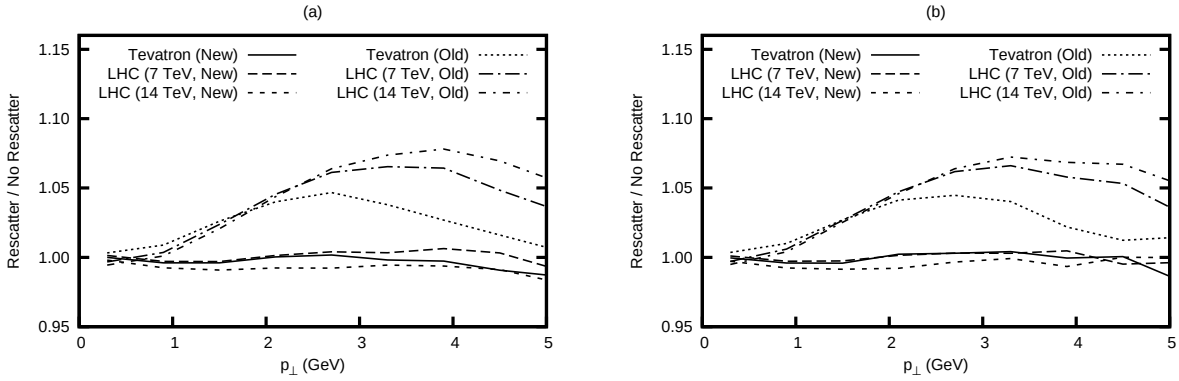

Figure 17: Ratio of rescattering to no rescattering for the production of (a) charged hadrons and (b) neutral pions for Tevatron and LHC minimum bias events ($p_\perp > 0.4\text{GeV}$, $|\eta| < 1.0$, old and new tunes)

range. Instead, for the old tune, we do indeed have an excess of partons in the upper-$p_\perp$ region after retuning. Towards the highest-$p_\perp$ scales, the ratios begin to return to unity; a result of the convolution of falling power-like ($\sim 1/p_\perp^4$) distributions. It is this excess of high-$p_\perp$ partons which we would expect to contribute to any Cronin type effect at the hadron level. The results for other energies and tunes are similar; it is only with the old tune where there is any visible enhancement in high-$p_\perp$ jet production.

Fig. 17 now shows the ratio of production with rescattering enabled to without rescattering for (a) charged hadrons and (b) neutral pions, for a range of different energies, both with the old and new tunes. As expected from the parton level study, it is only with the old tune that there are visible changes. The energy dependence of the different curves reflects the increased phase space for MPI (and therefore rescattering) at higher energies.

Most surprising is the lack of enhancement when the new tune is used. At Tevatron energies, this is not an obvious result, as this is the source of a large amount of the data used to tune the MPI model. This shows, then, one of the difficulties in tuning an event generator; contributions can be shifted around between the different models through parameter

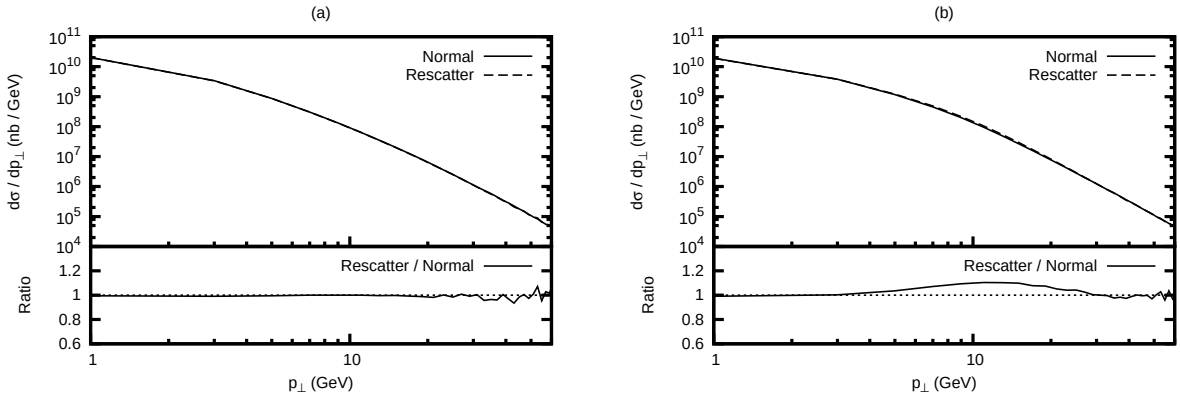

Figure 18: Inclusive jet $p_\perp$ distribution for LHC minimum bias events (pp, $\sqrt{s} = 14\,\text{TeV}$), (a) new tune, (b) old tune. The results with rescattering switched on are almost indistinguishable from the normal curves, but with the old tune the ratio does show a slight excess

adjustments (in this case a change in the hadronic matter profile and a slight change in $p_{\perp 0}$ and other parameters), such that the same data can be described in different ways. We have also seen that the underlying cause is the lack of high-$p_\perp$ enhancement at the parton level, but an interesting question is how, after retuning, the overall lower multiplicity at the parton level (Fig. 16) leads to the same average charged multiplicity at the hadron level. Most likely it is related to the more complicated colour flows that result from rescattering. This then ties in with the issue of colour reconnections, as discussed in the previous section, and as such we do not currently study this further.

5.4 Jet Study

Finally, we turn to a "jet" study of rescattering. We feed the hadron-level results of Pythia ($|\eta| < 3.5$, $p_\perp > 0.4\,\text{GeV}$) into FastJet and use the anti-$k_\perp$ algorithm ($R = 0.4$) [47]. When rescattering is enabled, the same $p_{\perp 0}$ values as Sec. 5.3 are used for simplicity.

The starting point is Fig. 16; at the parton level, with the old tune, we have seen an excess of high-$p_\perp$ partons, so we aim to see if this is also true after hadronisation. In Fig. 18, the inclusive jet distribution is shown for those jets with $|\eta| < 1.0$ for LHC minimum bias events (pp, $\sqrt{s} = 14\,\text{TeV}$, new and old tunes). The results follow the expected pattern; with the old tune, there is an excess of higher-$p_\perp$ jets, while with the new tune, there is almost no change.

We now extract the two-, three- and four-jet exclusive cross sections, where all jets must lie within $|\eta| < 1.0$ and have a minimum transverse momentum $p_{\perp\text{jet}} > 12.5\,\text{GeV}$. From Fig. 18, we see that it is with this $p_\perp$ cut that we expect the greatest rise in the different jet rates, and this is shown in Fig. 19 for the old tune as a function of the summed $p_\perp$ of the jets. There is a clear rise in the jet cross sections. Although, in itself, this is not any kind of definitive signature of rescattering, it is still encouraging. Rescattering does produce noticeable effects which will affect e.g. a full tuning of the generator.

As a final step, we check for kinematical signatures of rescattering. With DPS, for example, the different pairwise interactions are clearly distinct and azimuthal distributions can be used as a distinguishing signature. Rescatterings are not distinct in this way. They

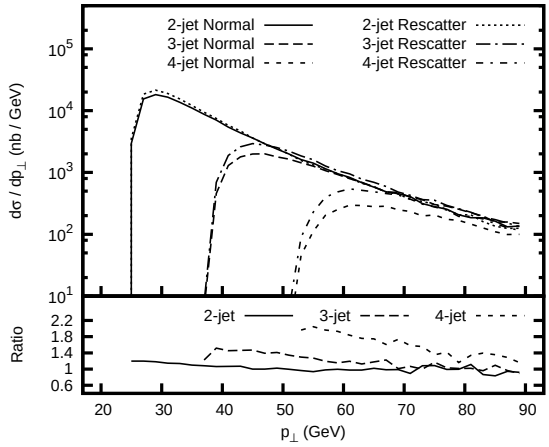

Figure 19: Two-, three- and four-jet exclusive cross sections for LHC minimum bias events (pp, $\sqrt{s} = 14\,\text{TeV}$, $p_{\perp\text{jet}} > 12.5\,\text{GeV}$, $|\eta| < 1.0$, old tune)

are very deeply entangled in the downward evolution of the final state, so it is not clear if any such signatures may exist. For the three-jet sample of Fig. 19, we study the smallest ΔR value between the different pairs of jets per event. One could hope that the distribution of ΔR values from three-jet events where rescattering is involved is somehow different than the background events (e.g. three-jet events from radiation which may be characteristically peaked in the small ΔR region). For the four-jet sample, we instead study the smallest and largest $\Delta\phi$ values between the jets per event. It is known that DPS events have a characteristic $\Delta\phi$ peak at π, but there are also radiative contributions which can mask rescattering. Unfortunately, for both samples, the results with and without rescattering are essentially indistinguishable.

6 Conclusions

In this article we have presented a model for rescattering in MPI, allowing the full generation of events from a central simple process to the multiparticle hadron-level final state. To the best of our knowledge, this is the first time that rescattering has been modeled in such a detailed manner. The model is implemented and available for public use inside the Pythia 8 event generator. The model—generator connection is very important here; MPI physics is so complicated, and hovering so near to the brink of nonperturbative physics, that purely analytical approaches have a limited range of validity.

The formalism outlined in Sec. 4.1 provides a method of including already scattered partons back into the PDFs of the hadron beams such that they can be rescattered. Further, in Sec. 4.2, we have shown that a natural kinematical suppression means that the importance of the different beam association procedures is reduced. The main technical challenges, then, come with the inclusion of radiation and beam remnants. The kinematics of a dipole-based parton shower, combined with the flow of colour from one scattering subsystem into another, can lead to potentially large momentum imbalances in those stages of event generation that use rotations and Lorentz boosts to adjust parton kinematics (namely ISR and primordial $k_\perp$). We have found that the "trick" of shifting the momenta of internal lines, to always

conserve system momentum, does not have large adverse effects on event generation and allows us to integrate rescattering fully into the existing framework.

As we have seen, rescattering is a common occurrence. At the LHC we predict that of the order of half of all minimum-bias events will contain at least one rescattering, and for events with hard processes the fraction is even larger. Nevertheless, evaluating the effects of rescattering is challenging since it is a secondary effect within the MPI machinery. The precise amount of MPI has to be tuned to data, e.g. by varying the $p_{\perp 0}$ turn-off parameter, so the introduction of rescattering to a large extent can be compensated by a slight decrease in the amount of "normal" $2 \to 2$ MPIs. Worse still, most MPIs are soft to begin with, and rescattering then introduces a second scale, even softer than the "original" scattering. Thus, rescattering is typically associated with particle production at the lower limit of what can be reliably detected. We have shown some effects of the Cronin type in hadronic $p_\perp$ spectra, but too small to offer a convincing signal.

If one zooms in on the tail of events at larger scales, the rate of (semi-)hard three-jet events from rescattering is of the same order in α_s as four-jets from DPS, but the background from initial- and final-state radiation starts one order earlier. Furthermore, DPS has some obvious characteristics to distinguish it from $2 \to 4$ radiation topologies: pairwise balanced jets with an isotropic relative azimuthal separation. No corresponding unique kinematical features are expected for rescattering and we have not found any new ones.

To some extent, this is a disappointing outcome of a project that has required the lengthy development of a complex, sophisticated machinery. However, let there be no doubt; rescattering is a logical consequence of MPI. In recent years, MPI has gained a wide acceptance, and come to be one of the cornerstones in our picture of hadronic physics. Therefore we can no longer rest content with qualitative estimates and models; we have to come up with quantitative answers to a number of detailed questions. The role of rescattering is one such, and certainly not the last one to need detailed modeling.

We should also not exclude that experimentalists may come up with new observables where rescattering is better visible, or tensions in the data that find an explanation with the presence of rescattering. Now that we can supply a complete implementation of rescattering, at least experimental studies will not be restricted by the theory support in this area. The next logical step, then, would be to produce full Pythia 8 tunes, with and without rescattering switched on (our procedure of only raising the $p_{\perp 0}$ parameter when rescattering is included is certainly too crude). Effects can then be studied across the range of observables used in tuning the generator, and changes to the parameters for the model with rescattering will give an insight into the role that it plays.

In the future we also hope to further improve our modeling. There are other areas left to address within the context of detailed models for MPI, such as the correlation between momentum fraction and transverse spread of partons in a hadron. Also areas not directly related to the MPI framework as such can be important, such as the colour reconnection procedure. There is such a hint of potential shortcomings in Sec. 5.3, where, with rescattering and the new tune, the parton-level multiplicity drops, and yet the hadron-level multiplicity stays the same.

So it is clear that this study is not the end of the story. Once the LHC starts, we can look forward to a wide range of new data on minimum-bias and underlying-event physics, which may further stimulate us to refine and rethink the MPI models used in current event generators. With rescattering, we have presented one possible future direction for models

and studies, which we hope can contribute towards a greater understanding of MPI at current and future colliders.

Acknowledgments

The authors wish to thank Florian Bechtel for his involvement in this project in an early phase.

This work was supported in by the Marie Curie Early Stage Training program "HEP-EST" (contract number MEST-CT-2005-019626) and in part by the Marie Curie research training network "MCnet" (contract number MRTN-CT-2006-035606).

For Feynman diagrams, Jaxodraw [48] was used.

References

[1] T. Sjöstrand and P. Z. Skands, *JHEP* **03** (2004) 053, arXiv:hep-ph/0402078.

[2] T. Sjöstrand and M. van Zijl, *Phys. Rev.* **D36** (1987) 2019.

[3] H.-U. Bengtsson and T. Sjöstrand, *Comput. Phys. Commun.* **46** (1987) 43.

[4] T. Sjöstrand, S. Mrenna, and P. Skands, *JHEP* **05** (2006) 026, arXiv:hep-ph/0603175.

[5] T. Sjöstrand and P. Z. Skands, *Eur. Phys. J.* **C39** (2005) 129–154, arXiv:hep-ph/0408302.

[6] M. Sandhoff and P. Skands. Presented at Les Houches Workshop on Physics at TeV Colliders, Les Houches, France, 2-20 May 2005.

P. Skands and D. Wicke, *Eur. Phys. J.* **C52** (2007) 133–140, arXiv:hep-ph/0703081.

[7] T. Sjöstrand, S. Mrenna, and P. Skands, *Comput. Phys. Commun.* **178** (2008) 852–867, arXiv:0710.3820 [hep-ph].

[8] R. Engel, *Z. Phys.* **C66** (1995) 203–214.

R. Engel and J. Ranft, *Phys. Rev.* **D54** (1996) 4244–4262, arXiv:hep-ph/9509373.

[9] **UA5** Collaboration, G. J. Alner *et al.*, *Nucl. Phys.* **B291** (1987) 445.

[10] G. Marchesini and B. R. Webber, *Phys. Rev.* **D38** (1988) 3419.

G. Marchesini *et al.*, *Comput. Phys. Commun.* **67** (1992) 465–508.

[11] J. M. Butterworth, J. R. Forshaw, and M. H. Seymour, *Z. Phys.* **C72** (1996) 637–646, arXiv:hep-ph/9601371.

[12] I. Borozan and M. H. Seymour, *JHEP* **09** (2002) 015, arXiv:hep-ph/0207283.

[13] M. Bähr, S. Gieseke, and M. H. Seymour, *JHEP* **07** (2008) 076, arXiv:0803.3633 [hep-ph].

M. Bähr *et al.*, *Eur. Phys. J.* **C58** (2008) 639–707, arXiv:0803.0883 [hep-ph].

[14] **Axial Field Spectrometer** Collaboration, T. Åkesson *et al.*, *Z. Phys.* **C34** (1987) 163.

[15] **CDF** Collaboration, F. Abe *et al.*, *Phys. Rev.* **D56** (1997) 3811–3832.

[16] **D0** Collaboration. D0 note 5910-CONF, http://www-d0.fnal.gov/Run2Physics/WWW/results/prelim/QCD/Q13/.

[17] **CDF** Collaboration, R. D. Field, `arXiv:hep-ph/0201192`.

[18] **CDF** Collaboration, R. Field and R. C. Group, `arXiv:hep-ph/0510198`.

[19] **CDF** Collaboration, R. D. Field. Presented at 33rd International Conference on High Energy Physics (ICHEP 06), Moscow, Russia, 26 Jul - 2 Aug 2006.

[20] **CDF** Collaboration, D. Kar, `arXiv:0905.2323 [hep-ex]`.

[21] Field, R.D., "recent talks available at http://www.phys.ufl.edu/ rfield/cdf/rdf_talks.html.".

[22] **UA1** Collaboration, C. Albajar *et al.*, *Nucl. Phys.* **B309** (1988) 405.

[23] P. Z. Skands, `arXiv:0905.3418 [hep-ph]`.

[24] A. Buckley, H. Hoeth, H. Lacker, H. Schulz, and J. E. von Seggern, `arXiv:0907.2973 [hep-ph]`.

[25] A. Moraes, C. Buttar, and I. Dawson, *Eur. Phys. J.* **C50** (2007) 435–466.

[26] N. Paver and D. Treleani, *Phys. Lett.* **B146** (1984) 252.
N. Paver and D. Treleani, *Z. Phys.* **C28** (1985) 187.

[27] E. Cattaruzza and D. Treleani, *Phys. Rev.* **D69** (2004) 094006, `arXiv:hep-ph/0401067`.

[28] J. Bartels, M. Salvadore, and G. P. Vacca, *Eur. Phys. J.* **C42** (2005) 53–71, `arXiv:hep-ph/0503049`.

[29] V. A. Khoze, A. D. Martin, and M. G. Ryskin, *JHEP* **05** (2006) 036, `arXiv:hep-ph/0602247`.

[30] E. Avsar, G. Gustafson, and L. Lönnblad, *JHEP* **01** (2007) 012, `arXiv:hep-ph/0610157`.

[31] C. Flensburg, G. Gustafson, and L. Lönnblad, *Eur. Phys. J.* **C60** (2009) 233–247, `arXiv:0807.0325 [hep-ph]`.

[32] G. Calucci and D. Treleani, *Phys. Rev.* **D79** (2009) 074013, `arXiv:0901.3089 [hep-ph]`.

[33] J. W. Cronin *et al.*, *Phys. Rev.* **D11** (1975) 3105.

[34] A. Donnachie and P. V. Landshoff, *Phys. Lett.* **B296** (1992) 227–232, arXiv:hep-ph/9209205.

[35] J. Dischler and T. Sjöstrand, *Eur. Phys. J. direct* **C3** (2001) 2, arXiv:hep-ph/0011282.

[36] G. Gustafson, L. Lönnblad, and G. Miu, *Phys. Rev.* **D67** (2003) 034020, arXiv:hep-ph/0209186.

[37] V. N. Gribov and L. N. Lipatov, *Sov. J. Nucl. Phys.* **15** (1972) 438–450.
G. Altarelli and G. Parisi, *Nucl. Phys.* **B126** (1977) 298.
Y. L. Dokshitzer, *Sov. Phys. JETP* **46** (1977) 641–653.

[38] V. V. Sudakov, *Sov. Phys. JETP* **3** (1956) 65–71.

[39] T. Sjöstrand, *Phys. Lett.* **B157** (1985) 321.

[40] M. Bengtsson, T. Sjöstrand, and M. van Zijl, *Z. Phys.* **C32** (1986) 67.

[41] G. Gustafson, *Phys. Lett.* **B175** (1986) 453.
G. Gustafson and U. Pettersson, *Nucl. Phys.* **B306** (1988) 746.
L. Lönnblad, *Comput. Phys. Commun.* **71** (1992) 15–31.

[42] S. Catani and M. H. Seymour, *Nucl. Phys.* **B485** (1997) 291–419, arXiv:hep-ph/9605323.

[43] H. Hoeth private communication, 2009.

[44] C. Buttar *et al.*, *HERA and the LHC - A workshop on the implications of HERA for LHC physics: Proceedings Part A* (2005) 192–217, arXiv:hep-ph/0601012.

[45] M. Glück, E. Hoffmann, and E. Reya, *Zeit. Phys.* **C13** (1982) 119.

[46] **CDF** Collaboration, T. Aaltonen *et al.*, *Phys. Rev.* **D79** (2009) 112005, arXiv:0904.1098 [hep-ex].

[47] M. Cacciari and G. P. Salam, *Phys. Lett.* **B641** (2006) 57–61, arXiv:hep-ph/0512210.
M. Cacciari, G. P. Salam, and G. Soyez, *JHEP* **04** (2008) 063, arXiv:0802.1189 [hep-ph].

[48] D. Binosi and L. Theussl, *Comput. Phys. Commun.* **161** (2004) 76–86, arXiv:hep-ph/0309015.